Atmospheric Environment 74 (2013) 259–276

Contents lists available at SciVerse ScienceDirect

Atmospheric Environment

journal homepage: www.elsevier.com/locate/atmosenv

Understanding of the formation mechanisms of ozone and particulate matter at a fine scale over the southeastern U.S.: Process analyses and responses to future-year emissions

Xiao-Huan Liu [a,b], Yang Zhang [b,*]

[a] Ocean University of China, Qingdao 266100, Shandong Province, PR China
[b] North Carolina State University, Department of Marine, Earth, and Atmospheric Sciences, Campus Box 8208, NCSU, Raleigh, NC 27695, USA

HIGHLIGHTS

- Fine scale (4-km) CMAQ modeling for an area in the southeastern U.S. in 2002/2018.
- Detailed process analysis to understand the formation mechanisms of O_3 and $PM_{2.5}$.
- Responses of future air quality and total N deposition to 2018 projected emissions.

ARTICLE INFO

Article history:
Received 22 January 2013
Accepted 29 March 2013

Keywords:
CMAQ
O_3
$PM_{2.5}$
Process analysis
Chemical regime indicators
Future-year air quality

ABSTRACT

Ozone (O_3) and fine particle ($PM_{2.5}$) formation over the southeastern U.S. are of a major concern due to high emissions of precursors and special weather conditions that are conducive to their formation. In this study, the Community Multiscale Air Quality (CMAQ) modeling system is applied to simulate the formation of major air pollutants over an area in the southeastern U.S. at a 4-km horizontal grid resolution for January, April, July, and October in 2002 and 2018. Model performance evaluation shows an overall satisfactory performance for O_3 in all months and for $PM_{2.5}$ in January and October at rural sites and in January, April, and October at urban sites. Large underpredictions in $PM_{2.5}$ concentrations occur in April and July at rural sites and in July at urban sites, because of biases in meteorological predictions and underestimation of emissions of precursors. The model performance at 4-km in terms of O_3, $PM_{2.5}$ and $PM_{2.5}$ components show some improvements but overall are not always better than that at 12-km. O_3 chemistry is VOC-limited in urban areas and NO_x-limited over the west of the mountain regions and the southern Georgia throughout the year, and VOC-limited over the rest of areas in January but NO_x-limited in other months. Among all photochemical indicators examined, $PH_2O_2/PHNO_3$ and O_3/NO_y are the most robust indicators. The domain is NH_3-rich or neutral in all months, indicating a high potential for NH_4NO_3 formation and the sensitivity of $PM_{2.5}$ formation to the emissions of SO_2, NO_x, and NH_3. Surface O_3 is accumulated primarily through vertical transport in urban, rural and coastal areas and both horizontal and vertical transport in mountain regions and produced via gas-phase chemistry at non-urban sites during daytime. The loss of O_3 is attributed to gas-phase chemistry via NO titration in urban areas, and dry deposition and transport processes in rural and mountain areas. $PM_{2.5}$ is produced by primary emissions and PM processes and lost through vertical and horizontal transport in urban areas. The combined effects of transport, emissions, and PM processes influence PM concentrations in other areas. The 2018 simulations project a decrease in $PM_{2.5}$ concentrations and an improvement in visibility over almost the entire domain, slight decreases in O_3 mixing ratios in urban areas in July and most non-urban areas in April and October but large increases in the rest of areas in other months, and a decrease in total N deposition fluxes in most areas except for central and eastern North Carolina and northern Georgia. The development of integrated emission control strategies should consider region-specific seasonality and differences in the responses of O_3, $PM_{2.5}$, visibility, and nitrogen deposition.

* Corresponding author.
E-mail address: yang_zhang@ncsu.edu (Y. Zhang).

1352-2310/$ – see front matter © 2013 Elsevier Ltd. All rights reserved.
http://dx.doi.org/10.1016/j.atmosenv.2013.03.057

1. Introduction

High ozone (O_3) and fine particulate matter ($PM_{2.5}$) levels and severe regional haze events featured with visibility degradation often occur in the southeastern U.S. High biogenic volatile organic compounds (BVOCs) emissions and hot humid summers with strong solar insolation and poor vertical mixing are major characteristics in this region, resulting in a NO_x-limited O_3 chemistry during summertime and the accumulation of air pollutants (Chameides and Cowling, 1995; Hansen et al., 2003; Zhang et al., 2006a, 2009; P. Liu et al., 2010). High emissions of sulfur dioxide (SO_2), ammonia (NH_3), BVOCs, and anthropogenic VOCs (AVOCs) lead to a dominance of ammonium sulfate and organic aerosol (OA) in observed $PM_{2.5}$ levels in this region during summertime (Hand et al., 2011).

Because of these special characteristics, the southeastern U.S. has been selected for several intensive field studies for regional photochemistry and aerosol formation including 1999 Southern Oxidants Study (SOS)/Nashville Study (Chameides and Cowling, 1995) and the upcoming Southern Oxidants and Aerosol Study (SOAS) and Southeast Nexus (SENEX) at Centreville (CTR), AL in summer 2013 (SOAS/SENEX white papers, http://wiki.envsci.rutgers.edu/index.php; http://esrl.noaa.gov/csd/projects/senex/). As a long-term observation and research program, the Southeastern Aerosol Research and Characterization Study (SEARCH) was initiated in mid-1998 to study the source, chemical speciation, and long-term trends of PM and gaseous concentrations in the southeastern U.S. (Hansen et al., 2003; Edgerton et al., 2006). A collaborative regional air quality monitoring and modeling program coordinated by the Visibility Improvement State and Tribal Association of the Southeast (VISTAS) was initiated in 2000 to support state implementation plans (SIP) for regional haze and related air quality issues over the southeast U.S. (http://www.vistas-sesarm.org). A number of air quality modeling studies have also been conducted over this region to understand the oxidant formation mechanisms and apportion major pollutant sources for O_3 and $PM_{2.5}$ in this area (e.g., Zhang et al., 2004, 2006b, 2009; Morris et al., 2006; Wu et al., 2008; Goldstein et al., 2009; X.H. Liu et al., 2010a; P. Liu et al., 2010; Liu and Zhang, 2010; Carlton et al., 2010; Burr and Zhang, 2011). In addition, air quality has been forecasted in real-time in this region using three-dimensional (3-D) air quality models (e.g., Odman et al., 2007; Chuang et al., 2011). Understanding the formation mechanisms of air pollutants is the key step toward air quality improvement for future years during which air quality may worsen due to population/economic growth and climate change.

The attainment of air quality and visibility standards for future years posts significant challenges in emission control technologies, regulation revision and enforcement, as well as decision tool development and application. 3-D air quality models, such as the U.S. EPA's Community Multiscale Air Quality (CMAQ) modeling system (Byun and Schere, 2006; Eder and Shaocai, 2006) are powerful tools for modeling current and future air quality. Process analysis (PA) embedded in CMAQ can be applied to identify dominant atmospheric processes for O_3 and $PM_{2.5}$ and the most influential reactions for their gaseous precursors. PA has been widely used for the pollutant formation mechanism study (e.g., Tonnesen and Dennis, 2000a; Yu et al., 2008, 2009; Zhang et al., 2009; X.H. Liu et al., 2010b; P. Liu et al., 2010). CMAQ has also been applied to simulate future air quality and its responses to future climate or emission changes either as a result of a changing climate or as part of emission control programs (e.g., Tagaris et al., 2007; Civerolo et al., 2008; Zhang et al., 2008, 2010).

In this work, CMAQ simulations with PA at a fine grid scale of 4-km over an area in the southeastern U.S. are conducted for four representative months in 2002 to simulate major air pollutants and investigate their governing chemical and physical processes. The simulation results at 4-km are evaluated using available observations and also compared with the VISTAS results at 12-km. CMAQ simulations with projected anthropogenic emissions for the year 2018 are also conducted to simulate the impact of projected emission changes on future air quality. The objectives of this work are to (1) understand the formation mechanisms and controlling processes of O_3 and $PM_{2.5}$; (2) evaluate the effectiveness of projected anthropogenic emission controls on future air quality in the southeastern U.S., and (3) compare the results at 4-km with those of VISTAS at 12-km to examine the sensitivity of the model predictions to different grid resolutions. At present, the SIP modeling is primarily performed at 12-km by VISTAS states (e.g., Morris et al., 2006). However, the U.S. EPA suggested that the SIP modeling may benefit from increased grid resolution from 12-km to 4-km, particularly over areas with high gaseous emissions and primary PM sources, (U.S. EPA, 2007). Previous studies showed that while O_3 is relatively insensitive to horizontal grid resolution, $PM_{2.5}$, deposition fluxes, visibility are moderately-to-significantly sensitive to grid resolution (Wu et al., 2008; X. H. Liu et al., 2010a) and the SIP modeling at different grid resolutions may give different results for attainment test (Zhang et al., 2010). The simulations at 4-km in this work would thus have added values to the SIP modeling.

2. Model setup and evaluation protocols

The MM5/CMAQ v4.5.1 simulations are conducted over an area covering nearly entire North Carolina (NC) and South Carolina (SC), northern Georgia (GA), and a small portion of adjacent states including Virginia (VA), Tennessee (TN), Kentucky (KY), Alabama (AL), and West Virginia (WV) at a 4-km horizontal grid resolution for January, April, July, and October in 2002 and 2018 (see Fig. S1 in the supplementary material). The vertical resolution is 19 layers extending from surface to the tropopause with about 38 m for the first layer. The meteorological and chemical initial and boundary conditions (ICs and BCs) for the 4-km MM5/CMAQ v4.5.1 simulations are generated based on the VISTAS MM5/CMAQ v4.5.1 simulation outputs over the eastern U.S. at 12-km. The emissions for the 4-km simulations are generated by applying the SMOKE version 2.1 to the same emission inventories of MACTEC (2008) that were used for the VISTAS 12- and 36-km simulations. To maintain a consistency in the model configurations for intercomparison of results at 4- and 12-km, the 4-km MM5/CMAQ simulations use the same configurations as those of the VISTAS 12-km simulations except for convective cloud treatments, which are turned off because all clouds are assumed to be resolved at a 4-km grid resolution. The projected anthropogenic emissions used for 2018 simulations are developed based on the 2002 emission inventory according to several emission control rules (MACTEC, 2008). The projected percentage changes in anthropogenic emissions of major emitted species in six major emission sectors in 2018 relative to their emission levels in 2002 for the seven states in the 4-km simulation domain are summarized in Table S1. Annual emissions of SO_2, nitrogen oxides (NO_x), VOCs, and carbon monoxide (CO) in 2018 are projected to reduce in those states by 43.0–70.3%, 43.1–59.2%, 17.5–35.1%, and 19.0–32.6%, respectively, those of NH_3, $PM_{2.5}$, and PM_{10} are projected to increase by 14.1–26.9%, 5.2–16.4% (except for West Virginia (WV) where the projected change is to decrease by 9.4%), and 2.4–24.3%, respectively. To study the impact of projected anthropogenic emission changes on future air quality, the 2002 meteorological inputs are used for the 2018 CMAQ simulations. The 2002 simulations are considered as the base simulations, which are used to evaluate the model performance against observations and also to investigate the formation mechanisms of O_3 and $PM_{2.5}$ using the PA tool in CMAQ. The 2018 simulations with projected

emissions are used to analyze the impacts of emission control on future air quality.

Simulated species concentrations and photochemical indicators in 2002 are evaluated with available observations. These observations include hourly O_3 mixing ratios from the Aerometric Information Retrieval System – Air Quality Subsystem (AIRS–AQS) and the Clean Air Status and Trends Network (CASTNET), 24-hr average concentrations of $PM_{2.5}$, $PM_{2.5}$ composition (ammonium (NH_4^+), nitrate (NO_3^-), sulfate (SO_4^{2-}), elemental carbon (EC), and organic carbon (OC), and total carbon (TC)) and visibility indices (haziness index (HI in deciview) and light extinction coefficient (β_{ext}, in Mm^{-1}) (1 data every 3 days) from the Interagency Monitoring of Protected Visual Environments (IMPROVE), 24-hr average concentrations of $PM_{2.5}$ and its composition (NH_4^+, NO_3^-, SO_4^{2-}, EC, and OC) (1 data every 3 or 6 days) from the Chemical Speciation Network (CSN), weekly 24-hr average concentrations of NH_4^+, NO_3^-, and SO_4^{2-} from CASTNET, the photochemical indicators (i.e., total reactive nitrogen (NO_y), O_3/NO_x, and O_3/NO_y) calculated based on hourly concentrations of NO_x, NO_y, and O_3 from SEARCH, weekly average dry deposition fluxes for NH_4^+, NO_3^-, and SO_4^{2-} calculated from the Multilayer Model (MLM) based on observed species concentrations and leaf area index recorded by CASTNET, and precipitation and wet deposition fluxes of NH_4^+, NO_3^-, and SO_4^{2-} from the National Acid Deposition Program (NADP). The AIRS–AQS, CSN, and SEARCH sites are mainly located in the urban and suburban areas while the CASTNET, IMPROVE, and NADP sites are mainly located in the rural and remote areas. Visibility degradation is the major characteristic of regional haze, and visibility improvement is the primary purpose of the VISTAS program. Visibility indices are calculated based on a mass reconstruction technique in CMAQ. HI is linear to humanly- perceived changes in visual air quality. One-unit change in HI is approximately a 10% change in β_{ext}, and is considered to be significant. β_{ext} indicates the attenuation of light per unit distance due to scattering and absorption by gases and particles in the atmosphere. For OC evaluation, a factor of 1.4 is used to convert simulated organic matter (OM) to OC (i.e., OM $\approx$ 1.4 OC) for its comparison with observed OC, and this value is likely to be an underestimation based on Turpin and Lim (2001). IMPROVE measures EC and OC based on the thermal optical reflectance protocol, consistent with the protocol used to estimate OC and EC emissions in the NEI. However, CSN measures EC and OC based on the thermal optical transmittance method, which is different from that of IMPROVE and CMAQ. To address this issue, TC, instead of separate EC and OC, at the CSN is used to evaluate simulated TC.

Model predictions are evaluated in terms of domainwide spatial distribution and performance statistics such as normalized mean bias (NMB) and normalized mean error (NME) as defined in Zhang et al. (2006a), temporal variation at specific sites, as well as seasonal variations. Six representative sites are selected for temporal evaluation including three urban sites (Jefferson Street (JST), Atlanta, GA, Charlotte (CHA), NC, and Raleigh (RAL), NC), one rural site (Yorkville (YRK), GA), one mountain site (Great Smoky National Park (GRS), TN), and one coastal site (Beaufort (BFT), NC). JST and YRK are the SEARCH sites, representing urban and rural areas where biogenic emissions are high. CHA and RAL are the NCDENR sites that have the highest O_3 and $PM_{2.5}$ concentrations in NC. The O_3 levels in Charlotte and Atlanta have been in moderate non-attainment based on the 1997 max 8-hr O_3 standard and marginal non-attainment based on the 2008 max 8-hr O_3 standard and the $PM_{2.5}$ level in Atlanta has been in non-attainment based on the 1997 $PM_{2.5}$ standard (http://www.epa.gov/oaqps001/greenbk/index.html). Charlotte and Atlanta rank the 10th and 23rd among the most polluted areas in terms of O_3 concentrations in the U.S. (American Lung Association, 2012). GRS and BFT are the CASTNET sites, and GRS is also an IMPROVE site. GRS and BFT represent less polluted areas but with complex terrains.

The PA tool in CMAQ includes the Integrated Process Rate analysis (IPR) and the Integrated Reaction Rate analysis (IRR). IPRs give the contributions of individual physical processes and the net effect of chemical reactions to the overall species concentrations. These processes include emissions of primary chemical species, gas-phase chemical reactions, horizontal transport (including diffusion and advection in both x and y directions), vertical transport (including diffusion and advection such as lower troposphere/boundary layer mixing and also transport from upper layers to boundary layers), cloud processes (including cloud attenuation of photolytic rates, convective and non-convective mixing and scavenging by clouds, aqueous-phase chemistry, and wet deposition), PM processes (including thermodynamic equilibrium of inorganic and organic species and dynamics such as homogeneous nucleation, condensation/evaporation, and coagulation), and dry deposition. IRRs give the contributions of individual chemical reactions to the net production and destruction rates of species concentrations. In this study, hourly IPRs are analyzed at 5 sites (i.e., JST, RAL, YRK, GRS, and BFT) over the southeast U.S. IRRs for 96 gas-phase reactions in the Carbon Bond Mechanism (CBM)-IV are calculated. The formation efficiency of O_3 and secondary PM is largely influenced by atmosphere oxidation capacity which can be indicated by the chemical production of total odd oxygen (Total_O_x_Prod) and OH chain length (OH_CL). OH_CL is the average number of times a newly-created OH radical cycle that is recreated through radical chain propagation before the OH radical is removed from the cycle through termination (Seinfeld and Pandis, 2006). Both Total_O_x_Prod and OH_CL are IRR outputs. Another IRR variable, the ratio of production rates of hydrogen peroxide (H_2O_2) and nitric acid (HNO_3), $PHNO_3/PH_2O_2$, is used to determine the VOC or NO_x-limited O_3 chemistry at a given site. In addition to $PHNO_3/PH_2O_2$, several indicators are calculated from CMAQ outputs, including total reactive nitrogen (NO_y), the ratios of H_2O_2/HNO_3, $H_2O_2/(O_3+NO_2)$, O_3/NO_x, O_3/NO_y, $HCHO/NO_2$, and $HCHO/NO_y$ (Sillman, 1995; Zhang et al., 2009). Secondary PM chemical regime (i.e., sensitivity of PM formation to changes of emissions of NO_x, SO_2, and NH_3) is also examined through three indicators: the degree of sulfate neutralization (DSN), gas ratio (GR), and adjusted gas ratio (AdjGR), as defined in the supplementary material. GR < 0 indicates NH_3-poor condition while GR > 1 represents NH_3-rich condition. The calculation of GR assumes that SO_4^{2-} is fully neutralized by NH_3, which may underestimate free NH_3 and NH_4NO_3 formation, particularly in cold weather (Pinder et al., 2008; Zhang et al., 2009). AdjGR is more robust than GR because it is defined based on DSN (instead of a full neutralization) and does not reply on this assumption. It can be applicable to conditions with insufficient neutralization of sulfate such as winter conditions. AdjGR has the same threshold values as GR.

3. Model evaluation

The VISTAS MM5 simulations at 12- and 36-km have been evaluated by Olerud and Sims (2004). VISTAS CMAQ simulations at 12- and 36-km have been evaluated by Morris et al. (2006). A brief summary of their evaluation is provided in the supplementary material. This work focuses on the evaluation of CMAQ predictions at 4-km. The biases and errors in MM5 and CMAQ simulations at 12- and 36-km will propagate into the 4-km MM5 and CMAQ simulations, respectively, performed in this work. In addition, those of MM5 simulations at 4-km will propagate into the 4-km CMAQ simulations in this work.

3.1. The 4-km simulation

Table 1 summarizes performances statistics for O_3, $PM_{2.5}$, $PM_{2.5}$ composition (i.e., SO_4^{2-}, NO_3^-, NH_4^+, EC, OC, and TC), visibility indices

Table 1
Performance statistics from the 4- and 12-km simulations for January, April, July, and October 2002.

Species	Network[a]	January			April			July			October		
		Data	NMB[b]	NME[b]	Data #	NMB	NME	Data #	NMB	NME	Data #	NMB	NME
Max 1-hr O_3	AIRS-AQS	384	4.6/4.7[c]	17.9/16.6	3030	2.1/6.1	12.1/12.6	3216	−12.6/−8.6	17.2/14.7	3185	5.1/17.7	20.8/25.3
	CASTNET	301	9.0/9.0	15.4/17.1	299	−6.9/−3.9	13.8/12.3	300	−8.8/−7.0	14.5/13.4	247	2.4/4.4	16.9/19.0
Max 8-hr O_3	AIRS-AQS	384	9.3/8.3	20.7/19.2	3027	3.3/8.6	13.0/14.2	3215	−10.1/−3.4	16.2/13.7	3183	10.9/25.5	23.8/31.0
	CASTNET	301	13.2/11.5	19.2/19.7	299	−1.8/1.1	12.4/11.8	300	−4.7/−1.0	14.5/14.2	246	6.9/15.3	18.6/23.5
24-hr avg. PM_{25}	IMPROVE	49	13.8/19.0	29.6/31.2	52	−33.0/−25.3	36.1/30.4	55	−57.8/−50.1	60.0/52.1	59	−0.4/21.2	32.9/39.9
	CSN	76	19.0/7.8	37.5/32.2	104	−18.5/−20.4	35.1/33.9	127	−49.6/−46.1	51.2/46.5	128	10.2/8.0	37.8/34.8
24-hr avg. SO_4^{2-}	IMPROVE	49	5.3/7.2	32.1/33.5	53	−26.0/−18.3	29.3/26.8	56	−39.1/−23.6	50.2/38.5	137	8.6/46.4	34.9/57.6
	CASTNET	39	−18.2/−21.2	22.6/25.3	39	−24.4/−20.7	25.1/22.9	40	−23.9/−12.3	26.9/17.5	35	−2.6/18.7	18.9/31.6
	CSN	79	−10.3/−17.7	39.3/39.8	120	−19.7/−19.9	36.8/34.4	135	−34.3/−18.0	44.4/31.7	137	−4.2/6.2	36.9/38.0
24-hr avg. NO_3^-	IMPROVE	49	45.5/38.7	104.9/88.5	53	1.6/−13.7	95.3/91.8	56	−61.8/−80.2	107.1/92.2	59	115.6/86.1	183.1/180.7
	CASTNET	39	1.6/13.1	54.6/59.8	39	−2.1/−4.2	65.7/64.1	40	−73.4/−81.4	89.7/86.6	35	118.8/103.0	169.6/161.8
	CSN	79	103.5/94.6	126.9/119.3	120	−5.8/−12.1	88.7/93.3	135	−86.9/−89.9	86.9/90.8	137	124.0/87.3	155.7/137.1
24-hr avg. NH_4^+	IMPROVE	—[d]	–	–	10	−11.9/−7.2	19.2/19.4	9	−57.3/−48.4	60.3/49.6	59	30.4/50.4	50.7/64.0
	CASTNET	39	−6.9/−1.9	25.0/22.7	39	−5.7/−5.6	16.0/15.0	40	−52.4/−50.3	52.4/50.5	35	11.3/17.3	27.7/31.0
	CSN	79	59.3/51.2	80.6/72.4	120	3.2/1.9	44.9/42.0	135	−41.2/−37.3	50.0/45.8	137	43.2/39.8	59.3/54.8
24-hr avg. EC	IMPROVE	49	−9.4/3.4	33.1/36.3	53	−40.2/−30.1	41.3/35.6	43	−46.6/−42.5	63.2/60.9	59	−40.5/−36.3	46.1/45.2
	CSN	79	2.4/−4.4	47.1/43.2	111	−21.9/−29.5	46.3/49.8	134	37.6/20.8	79.9/75.5	137	7.7/−11.5	55.0/44.6
24-hr avg. OC	IMPROVE	49	−15.1/−4.3	30.9/34.2	53	−51.4/−41.2	51.4/43.9	43	−72.5/−70.3	75.8/73.6	59	−52.1/−49.2	54.9/52.6
24-hr avg. TC	IMPROVE	43	−14.0/−3.5	28.9/32.6	53	−49.6/−39.5	49.6/42.3	43	−69.6/−67.1	73.8/71.6	59	−50.3/−47.1	52.7/50.6
	CSN	79	−49.7/−51.9	52.4/53.5	111	−54.0/−57.5	55.3/58.8	134	−73.3/−75.9	74.6/76.4	132	−50.5/−56.8	56.8/58.6
β_{ext} (Recon)	IMPROVE	42	96.0/56.3	119.6/77.5	46	−10.4/−13.0	41.6/31.8	32	−50.3/−39.4	57.8/49.9	59	84.5/68.1	101.1/74.4
HI (Recon)	IMPROVE	42	−4.4/−6.4	27.3/22.0	46	−28.3/−23.9	30.7/25.9	32	−40.3/−29.3	41.0/30.5	59	2.4/7.2	26.7/20.3
DD_NH_4^+[e]	CASTNET	6450	−68.0/−71.8	86.7/83.9	6785	−76.4/−74.6	80.8/79.4	6239	−89.0/−88.2	96.2/88.9	6594	−65.2/−66.3	83.7/80.4
DD_SO_4^{2-}	CASTNET	6450	−55.7/−72.0	96.6/82.9	6785	−79.0/−76.8	83.8/81.9	6239	−80.1/−75.4	96.8/78.6	6594	−61.5/−62.9	90.0/80.7
DD_NO_3^-	CASTNET	6450	−63.2/−70.3	102.1/94.1	6785	−80.3/−77.8	93.1/92.3	6239	−98.0/−98.4	99.7/99.6	6594	−43.2/−48.4	112.4/108.6
WD_NH_4^+[e]	NADP	62	14.7/1.8	68.9/58.1	57	29.4/20.2	77.1/67.8	68	18.8/4.0	106.4/87.5	76	19.0/3.6	69.1/79.7
WD_SO_4^{2-}	NADP	62	12.7/−3.8	51.4/42.1	57	25.3/26.4	69.0/62.0	68	46.5/30.3	120.9/96.5	76	13.3/2.9	67.2/76.1
WD_NO_3^-	NADP	62	51.8/34.8	81.0/69.6	57	0.4/−18.6	72.0/55.1	68	−34.9/−45.8	75.9/69.5	76	38.1/11.0	80.8/81.9
Daily Precip	NADP	72	−10.9/−4.0	40.1/31.6	80	19.1/39.6	76.7/88.7	84	148.5/110.7	199.0/149.4	84	−30.1/−34.6	61.1/63.1

[a] AIRS–AQS: the Aerometric Information Retrieval System – Air Quality Subsystem; CASTNET: the Clean Air Status and Trends Network, IMPROVE: the Interagency Monitoring of Protected Visual Environments, CSN: the Chemical Speciation Network, and NADP: the National Acid Deposition Program.
[b] NMB – Normalized mean bias, %; NME – Normalized mean error, %.
[c] A/B- read A as the statistics from the 4-km simulation and B as the statistics from the 12-km simulation.
[d] No observational data available.
[e] DD – dry deposition and WD – wet deposition.

(β_{ext} and HI), dry and wet deposition fluxes of NH_4^+, SO_4^{2-}, and NO_3^- (DD_SO_4^{2-}, DD_NO_3^-, DD_NH_4^+, and WD_SO_4^{2-}, WD_NO_3^-, WD_NH_4^+, respectively) and precipitation (Precip). Fig. S1 shows simulated spatial distributions overlaid with observations in the 4 months in 2002 for max 1-h and 8-h average O_3 and 24-h average $PM_{2.5}$. Both max 1-h and 8-h O_3 mixing ratios at urban and rural sites are slightly overpredicted (NMBs of 2.1–10.9%) in January, April, and October and moderately underpredicted (NMBs of −12.6% to −10.1%) in July, indicating an overall satisfactory model performance based on criteria for model performance recommended by U.S. EPA (U.S. EPA, 2007) and several studies (e.g., Eder and Shaocai, 2006; Zhang et al., 2006a). The model simulations moderately-to-significantly underpredict $PM_{2.5}$ concentrations in April and July at urban and rural sites (NMBs of −26.0% to −18.5% and −57.8% to −49.6%, respectively), and overpredict them in January (NMBs of 13.8–19.0%) and October (an NMB of 10.2% at the CSN sites), with the worst performance in July. Figs S2 and S3 show temporal variations of observed and simulated surface O_3 mixing ratios at JST, YRK, CHA, RAL, GRS, and BFT and $PM_{2.5}$ concentrations at all sites except for BFT where no $PM_{2.5}$ observations are available. While CMAQ generally performs well for O_3 at these sites, large overpredictions at CHA and RAL in January and large underpredictions at all sites in July occur in $PM_{2.5}$ concentrations. The underpredictions may be attributed to possible underestimation in the emissions of gaseous precursors of secondary $PM_{2.5}$ (e.g., SO_2, NO_x, NH_3, and VOCs) and emissions of primary $PM_{2.5}$ species such as OC and EC, particularly in urban areas as reported in the work of Zhang et al. (2006c), P. Liu et al. (2010), and Liu and Zhang (2010), and overpredictions in precipitation that leads to overpredictions in the removal of SO_4^{2-} through wet deposition. Incomplete model treatments such as precursors and formation pathways for secondary organic aerosol (SOA) may also contribute to underpredictions of $PM_{2.5}$ (Morris et al., 2006), although CMAQ v4.5.1 used in this work already includes a more advanced SOA module than the EPA's released version of CMAQ v4.5.1. The overpredictions in January and October are attributed to a weaker than actual vertical mixing simulated by CMAQ as reported in Olsen (2009).

Among $PM_{2.5}$ components, model performance for NO_3^- is the worst, especially in July and October, with NMBs of −86.9% to −61.8% and 115.6%–124.0%. The significant biases in NO_3^- predictions can be attributed to several factors including uncertainties in precursor emissions (i.e., emissions of NO_x and NH_3 may be underestimated in July but overestimated in October), the errors in simulated SO_4^{2-} and NH_4^+ (Yu et al., 2005), and inaccuracies in simulated meteorological conditions (e.g., precipitation is significantly overpredicted with an NMB of 148.5%). In addition, large uncertainties exist in the observed concentration of NO_3^- due to its volatility (Zhang et al., 2010). Semi-volatile components such as nitrate and organics are expected to decrease as they shift from the particulate phase to the gas phase at higher temperatures. Although the heterogeneous reaction of N_2O_5 was considered in CMAQ, other missing heterogeneous reactions of nitrogen species such as HONO on the surface of particles may be another reason for the underprediction of NO_3^-. Model performance for SO_4^{2-} is better than NO_3^-, with NMBs of −39.1% to 8.6% at all sites. The concentrations of NH_4^+ at rural sites are underpredicted in January, April, and July (NMBs of −57.3% to −5.7%) but overpredicted in October (NMBs of 11.3%–30.4%). At urban sites, overpredictions occur in

January, April, and October (NMBs of 3.2–59.3%) but underpredictions remain in July (NMB of −41.2%), due likely to inaccuracies in NH_3 emissions and overpredictions in precipitation (particularly in July). Model predictions for EC have relatively small bias at the IMPROVE sites in January and at the CSN sites in January and October but larger biases in other months. As compared to EC, OC performance is slightly worse at the IMPROVE sites. TC is slightly underpredicted at the IMPROVE sites in January but significantly underpredicted at the IMPROVE sites in other months and at the CSN sites in all months. The underestimated emissions of EC and primary OC and the underpredicted SOA are major factors for the underpredictions in those carbonaceous species. β_{ext} is significantly overpredicted in January and October and moderately underpredicted in April and July. HI agrees well with observations in January and October and moderately underpredicted in April and July. Moderate-to-large underpredictions occur in DD_SO_4^{2-}, DD_NO_3^-, and DD_NH_4^+ in all months. Despite underpredictions in Precip in January and October, slight-to-moderate overpredictions occur for WD_SO_4^{2-}, WD_NO_3^-, and WD_NH_4^+, indicating that the impact of ambient concentrations of these species dominates over the impact of Precip in wet deposition fluxes. Precip is moderately and significantly overpredicted in April and July, respectively. The large overpredictions in Precip in July are attributed to the limitation of MM5 in capturing convective rainfall in terms of its frequency and intensity (Olerud and Sims, 2004). Slight-to-moderate overpredictions occur for WD_SO_4^{2-}, and WD_NH_4^+ in both months and for WD_NO_3^- in April, indicating that the impact of Precip dominates in both months. In July, WD_NO_3^- is moderately underpredicted, because of a significant underprediction in the concentrations of NO_3^-, possibly resulted from inaccurate emissions of NO_x (e.g., missing lighting emissions of NO_x, Appel et al., 2011). The relative importance of chemical concentrations and precipitation in determining wet deposition fluxes in winter and summer months is consistent with the finding of Queen and Zhang (2008).

Fig. 1 compares simulated and observed photochemical indicators (i.e., NO_y, O_3/NO_x, and O_3/NO_y) during afternoon hours (2–6 pm) at two SEARCH sites (JST and YRK) in the four months. Based on the original transition values proposed for these indicators, the values of $NO_y < 10–25$ ppb or 20 ppb (Milford et al., 1994; Sillman, 1995), $O_3/NO_x > 15$ (Tonnesen and Dennis, 2000b), and $O_3/NO_y > 7$ (Sillman et al., 1997) indicate a NO_x-limited O_3 chemistry, otherwise O_3 chemistry is VOC-limited. However, uncertainties exist in those threshold values. Alternative or adjusted values have been proposed (e.g., Lu and Chang, 1998; Zhang et al., 2009; X. H. Liu et al., 2010b). For example, Zhang et al. (2009) suggested adjusting them from 20 to 5 for NO_y, from 7 to 15 for O_3/NO_y, and from 15 to 60 for O_3/NO_x over continental U.S., which may be more suitable than the originally proposed threshold values. Some influential factors for different threshold values have been identified. For example, some of the original transition values were developed according to limited field measurements or different atmospheric conditions or model simulations with different mechanisms and horizontal grid resolutions (Zhang et al., 2009; X.H. Liu et al., 2010b). Therefore, a need to adjust the transition values of these indicators is warranted, and more indicators or more robust indicators should be used to distinguish NO_x and VOC-limited conditions which will be discussed in Section 4.2.

At JST, based on adjusted thresholds, both simulated and observed values show $NO_y > 5$ ppb, $O_3/NO_x < 60$ ppb and $O_3/NO_y < 15$ ppb in all months, indicating that JST has VOC-limited O_3 chemistry. This is also generally consistent with the result based on the originally proposed thresholds except that O_3 chemistry is NO_x-limited based on NO_y on 40%, 70%, and 20% of days in April, July, and October, respectively. Simulated NO_y are higher (much higher during some hours) and simulated O_3/NO_x and O_3/NO_y are lower than observations in the four months at JST. Simulated and observed indicators agree well at YRK. Most observed NO_y values for January and October are $\geq$5 ppb, while O_3/NO_x and O_3/NO_y are lower than the adjusted thresholds of 60 and 15, respectively, suggesting a VOC-limited O_3 chemistry at YRK. Unlike January and October, the O_3 chemistry is VOC-limited on some days and NO_x-limited on some days in April and July. When the original thresholds are used at YRK, inconsistencies exist among three indicators, e.g., NO_y are below 20 ppb on 95% of days in the four months, indicating a NO_x-limited O_3 chemistry. However, O_3/NO_x and O_3/NO_y are not higher than their thresholds of 15 ppb and 7 ppb on some days, particularly in January and October, indicating a VOC-limited O_3 chemistry.

3.2. The 12-km simulation and its comparison with the 4-km simulation

Table 1 also shows performance statistics from the 12-km simulations over the 4-km simulation domain. O_3 performance at 12-km is better in July but generally worse than that at 4-km in other months, particularly in October, indicating the benefit from the use of a finer grid resolution of 4-km. Simulated $PM_{2.5}$ concentrations at 4-km are better than or similar to those at 12-km in all months except for October at the IMPROVE sites and in all months except for January at the CSN sites. Comparing with the 12-km simulations, $PM_{2.5}$ predictions at 4-km are much closer to the observations at the IMPROVE sites in October (NMBs of −0.4% vs. 21.2%) and worse at the CSN sites in January (NMBs of 19.0% vs. 7.8%). For $PM_{2.5}$ components, similar to the simulations at 4-km, the performance of NO_3^- is the worst at 12-km. The simulated NO_3^- concentrations are closer to the observations at 12-km in January and October but worse in April and July at all sites. Predicted SO_4^{2-} concentrations at 12-km are closer to the observations than at 4-km or comparable to those at 4-km in April and July at all sites, but they are worse in January and October. For NH_4^+ concentrations, the model performs better at 12-km in January, April, and July at all sites but worse in October at the IMPROVE and CASTNET sites. For EC, the model performs slightly better at 12-km at the IMPROVE sites for all months but slightly worse at the CSN sites in all months except for July. For OC, the model at 12-km performs slightly better at the IMPROVE sites in all months. For TC, the model at 12-km performs slightly better at the IMPROVE sites but slightly worse at the CSN sites in all months. The model performance statistics at 4-km in terms of $PM_{2.5}$ and its components show some improvements but overall are not always better than that at 12-km, consistent with previous studies in this area (e.g., Arunachalam et al., 2006; Wu et al., 2008; Queen and Zhang, 2008). Compared with the 4-km simulation, the 12-km simulation gives overall better performance for β_{ext} and either similar or better performance for HI in all months, slightly better performance in dry deposition in April and July but worse performance in January and October for all species, better performance in WD_NH_4^+ for all months, WD_SO_4^{2-} for January, July, and October, and WD_NO_3^- for January and October, and also better performance in Precip in January and July. A more detailed assessment of model sensitivity to different horizontal grid resolutions (12-, 4-, and 1.33-km) can be found in Olsen (2009).

4. Process analysis

4.1. Controlling processes for chemical species at surface

Figs. 2 and 3 show the daily-mean hourly contributions of individual process to the concentrations of surface O_3 and $PM_{2.5}$, respectively, at JST, YRK, RAL, GRS, and BFT. Although these results

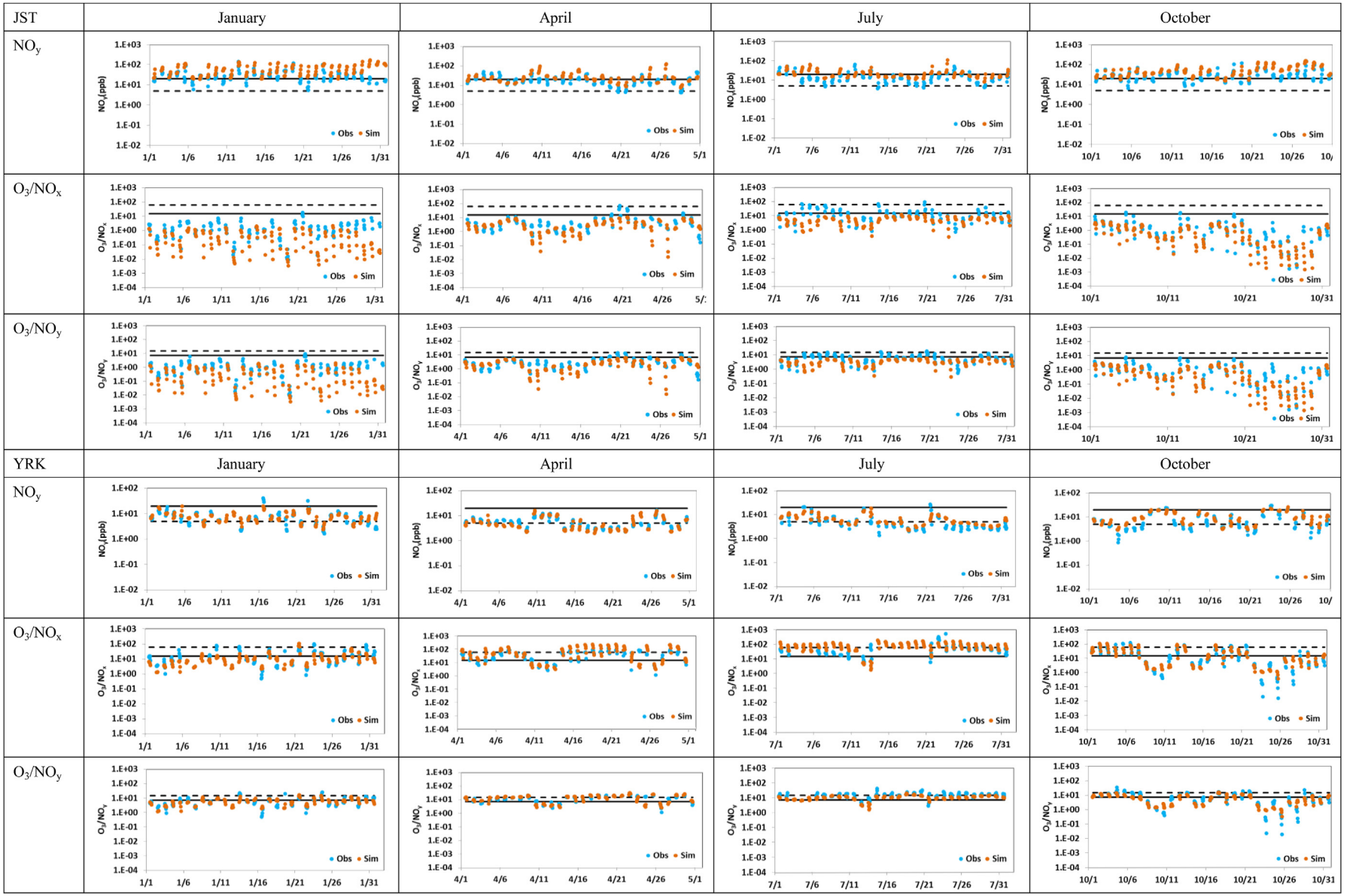

Fig. 1. Observed vs. simulated photochemical indicators at JST and YRK in 2002. The solid and dash lines indicate the original and adjusted threshold values.

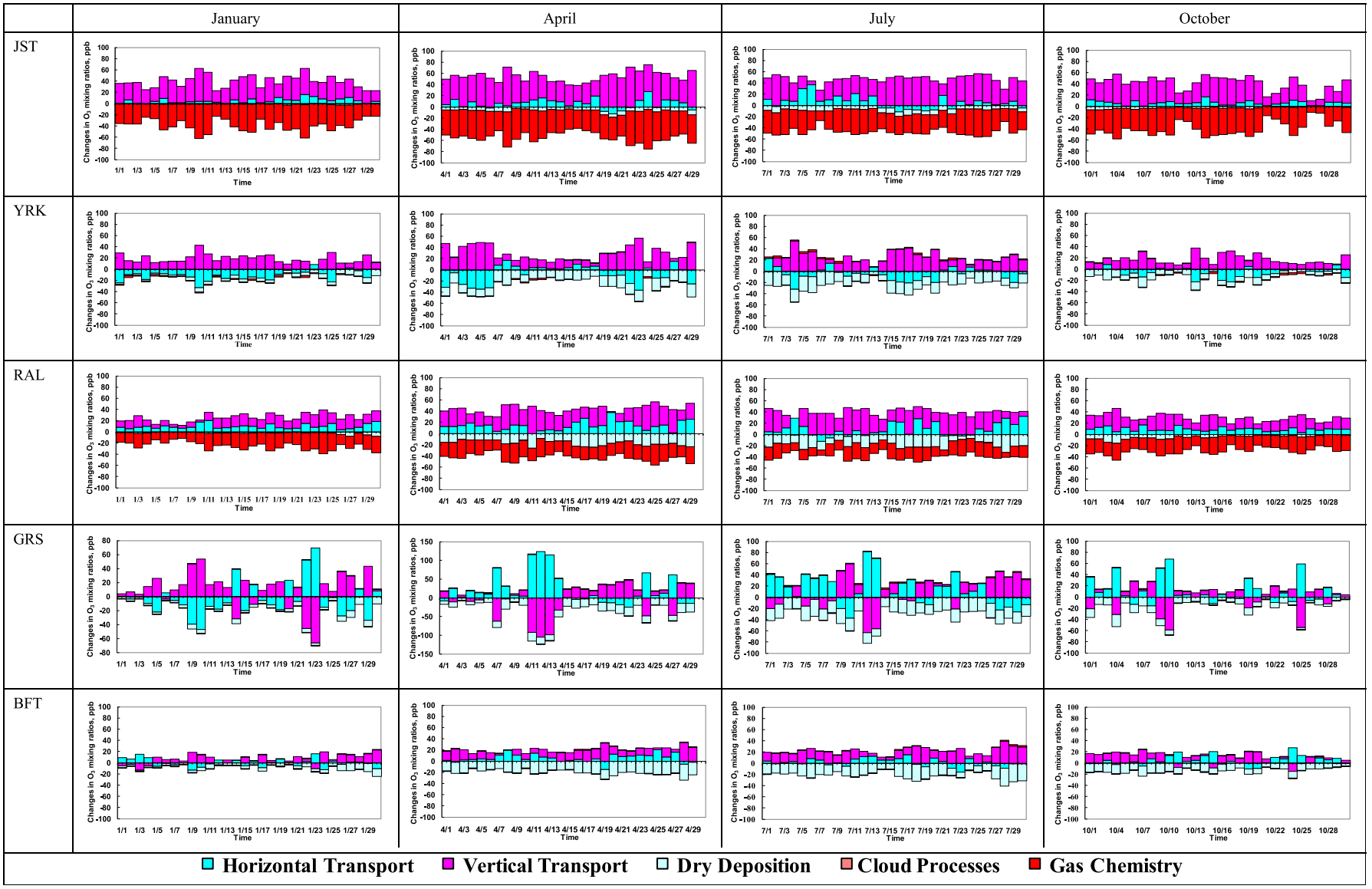

Fig. 2. Daily-mean hourly contributions of individual processes to the surface mixing ratios of O_3at 5 sites (Jefferson Street (JST), Atlanta, GA; Yorkville (YRK), GA; Raleigh (RAL), NC; Great Smoky National Park (GRS), TN; and Beaufort (BFT), NC) in the southeastern U.S. in January, April, July, and October 2002.

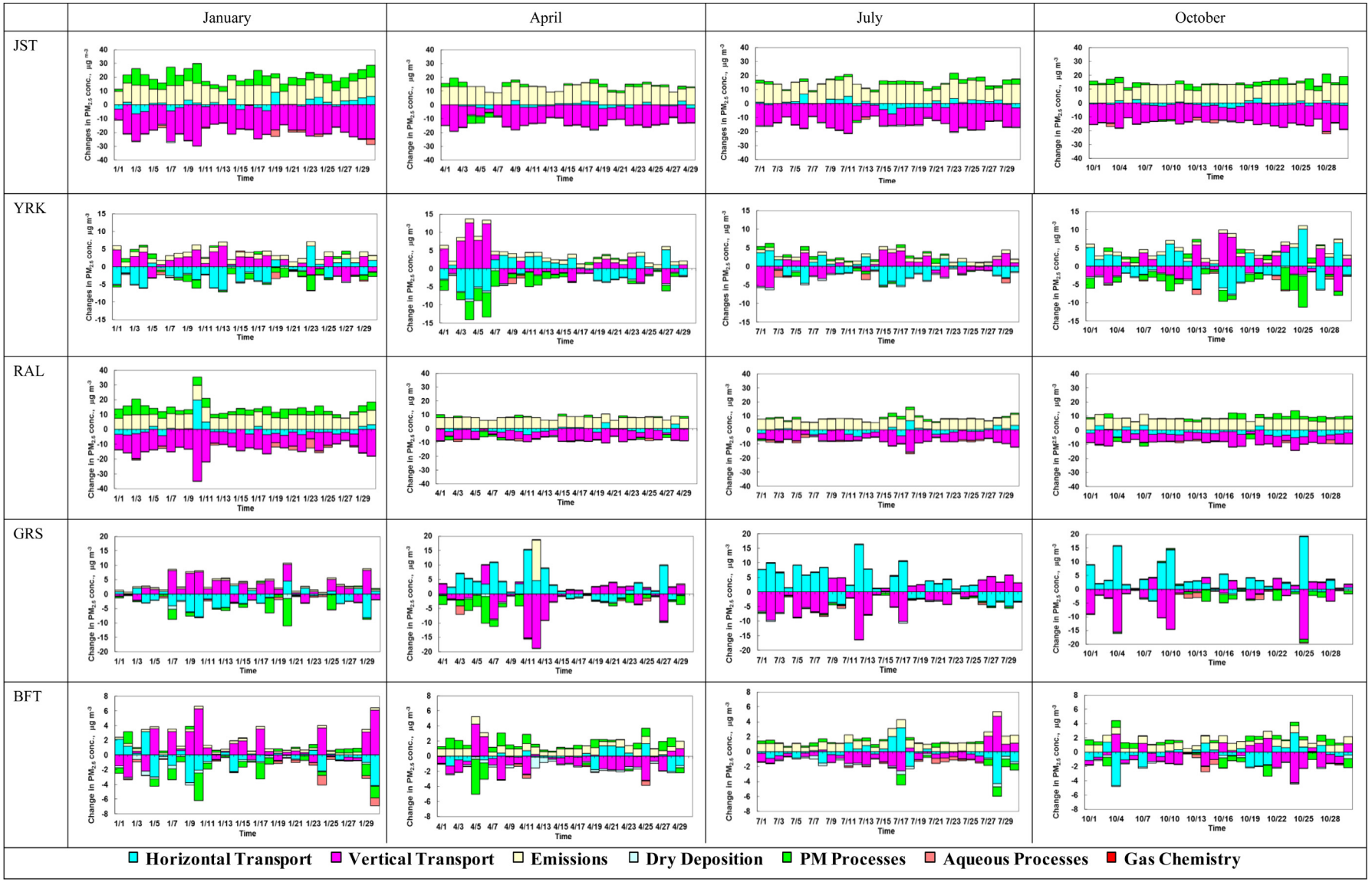

Fig. 3. Daily-mean hourly contributions of individual processes to the surface concentrations of PM_{25} at 5 sites (Jefferson Street (JST), Atlanta, GA; Yorkville (YRK), GA; Raleigh (RAL), NC; Great Smoky National Park (GRS), TN; and Beaufort (BFT), NC) in the southeastern U.S. in January, April, July, and October 2002.

cannot be verified because of lack of observations, they provide insights into the dominant formation mechanisms for O_3 and $PM_{2.5}$. High NH_3 emissions would impact $PM_{2.5}$ via its neutralization by H_2SO_4 and HNO_3. Therefore, similar figures are shown for NH_3, HNO_3, NH_4^+, and NO_3^-, in the supplementary material (Figs S4–S7). In addition, the monthly-mean diurnal contributions of individual process to the surface mixing ratios of O_3 and other gaseous precursors of O_3 and $PM_{2.5}$ including NO, NO_2, VOCs, SO_2, and NH_3 are shown in Fig. 4 and those for the surface concentrations of $PM_{2.5}$ and its major composition including NH_4^+, SO_4^{2-}, NO_3^-, EC, and OM are shown in Fig. 5 at JST and YRK. Daily-mean IPR analyses in Fig. 2 show that vertical transport plays a dominant role in transporting O_3 in urban (JST and RAL), rural (YRK), and coastal (BFT) areas, while the contributions from horizontal transport to O_3 mixing ratios are larger than vertical transport in the Mountain (GRS) region. The diurnal behavior analyses in Fig. 4 show that gas-phase chemistry contributes to O_3 production from 8 am to 7 pm and destruction at night in non-urban areas such as YRK, BFT, and GRS. In contrast, at urban sites where NO emissions are high, gas-phase chemistry is a dominant pathway to remove O_3 via NO titration during all hours in a typical day (see Fig. 4 at JST). Dry deposition and/or vertical/horizontal transport decrease most O_3 at other sites. As shown in Fig. 4, the diurnal variation of process contributions of O_3 is driven by that of its major precursors. At an urban site, JST, while freshly-emitted NO is converted to NO_2 which produces O_3, such a production is compensated by O_3 destruction though titration of NO, leading to a net O_3 loss by gas-phase chemistry throughout the day in July 2002. For comparison, at YRK, O_3 titration by NO still occurs during all hours but to a much less extent, which is compensated by O_3 production following the formation of NO_2 during 8 am to 7 pm, leading to a net O_3 formation via gas-phase chemistry. The fate of VOCs, another important precursor of O_3, is controlled primarily by emissions and vertical transport at JST and YRK. The contributions of other processes such as horizontal transport, gas-phase chemistry, and dry deposition are relatively small. The process analysis of O_3 and its major precursor at surface shows importance of transport, gas-phase chemistry, and dry deposition. Cloud processes are shown to be secondary important in the episodes simulated in this work.

As shown in Fig. 3, primary emission is a dominant source for $PM_{2.5}$ production in urban areas. As shown in Fig. 5, PM processes can contribute to PM production most of hours on an average day in July 2002 at urban sites. Vertical transport is a dominant sink at all urban sites. Horizontal transport can contribute to both gain and loss of $PM_{2.5}$ at all sites. Cloud processes remove $PM_{2.5}$ on a few days at all sites. At rural and coastal sites, primary emissions contribute to $PM_{2.5}$ production, vertical transport, horizontal transport, and PM processes may contribute to $PM_{2.5}$ gain or loss, depending on meteorological and chemical conditions at individual sites. For example, at YRK, PM processes can contribute to PM production mainly at nighttime and late evening in July 2002 (see Fig. 5). At GRS, the contribution of primary emissions to PM concentration is negligible, horizontal and vertical transport are dominant processes that influence PM concentrations in all months, and PM processes contribute to its loss on some days in January and April. Figs S4–S7 show daily-mean hourly contributions of individual processes to the mixing ratios of NH_3 and HNO_3 and the concentrations of NH_4^+ and NO_3^- at the surface. The dominate processes vary from species to species. For a primary species such as NH_3, emissions are the largest contributor to NH_3 at most sites and removal processes include PM processes, vertical transport, and dry deposition. For secondary gaseous species such as HNO_3, dominant sources at urban sites include gas-phase chemistry and vertical transport, and dry deposition is the primary removal pathway. For secondary inorganic species such as NH_4^+ and NO_3^-, PM processes, or transport, or a combination of two may contribute to their gain or loss, depending on locations. A more detailed analysis can be found in the Supplementary material. Comparisons among different forms of nitrogen (N), i.e., NH_4^+, NO_3^-, HNO_3, and NH_3 at different sites show that, dry deposition fluxes of HNO_3 and NH_3 are more significant than those of NH_4^+ and NO_3^- at all sites, indicating their dominance in the total N deposition over the southeastern U.S. (see more detailed discussions in Section 6). High rates of NH_3 deposition are found at RAL, JST, and YRK where the emissions of NH_3 are relatively high, indicating that dry deposition is an important sink (in addition to vertical transport) at these locations. These results are consistent with findings of Dennis et al. (2010). HNO_3 deposition rates are high at most sites in all months, especially at YRK, BET, and GRS in January and October, and at JST and RAL in April, July, and October.

The diurnal behavior of controlling processes of additional gaseous precursors of secondary PM such as SO_2 and NH_3 at JST and YRK is shown in Fig. 4. The production of SO_2 is dominated by primary emissions at JST but a combination of emissions and vertical and horizontal transport at YRK. SO_2 is vented out of this area primarily by vertical transport on all hours, in particular, daytime at JST and by horizontal transport during nighttime and evening at YRK. Dry deposition is an important removal process at both sites, particularly at YRK. As shown in Fig. 5, the amount of SO_2 that is converted to H_2SO_4 through gas-phase chemistry followed by the condensation of H_2SO_4 contributes to SO_4^{2-} formation at both sites. Primary emissions produce most NH_3 during all hours, and several processes such as vertical transport, PM processes, or dry deposition remove most NH_3 with higher removal rates during daytime than nighttime at both sites. The amount of NH_3 removed by PM processes is converted to NH_4^+, as shown in Fig. 5. NO_3^- losses due to evaporation at both sites during daytime or at YRK even during some nighttime/evening hours when temperatures remain high. It forms through gas-to-particle conversion processes during nighttime and evening at JST. EC and OM are mainly produced by emissions and removed by vertical transport on all hours at JST. PM processes can produce SOA (which contributes to OM) at night but reduce SOA during daytime due to volatility of SOA at YRK. At YRK, emissions on all days and horizontal transport on most days contribute to the production of EC. The removal processes of EC include vertical transport, dry deposition, and cloud processes. For OM at YRK, it is produced by emissions and vertical transport during daytime and PM processes at night. PM processes act to remove OM during daytime, and horizontal and vertical transport contribute to its loss at night. However, because of the incomplete treatments for SOA in CMAQ which results in a significant underprediction of OM (see Table 1), CMAQ may have underestimated the contributions of PM processes to OM formation in the southeastern U.S., particularly during the daytime in summer when the observed OM concentrations are similar to those at night reported in Baek et al. (2011).

4.2. Sensitivity of O_3 formation and atmospheric oxidation capacity

Fig. 6 shows the spatial distributions of monthly-mean $PH_2O_2/PHNO_3$ and Total_Ox_Prod obtained from the IRR output and O_3/NO_y calculated based on CMAQ predictions. Fig. S8 shows similar plots for additional O_3 sensitivity indicators calculated based on CMAQ outputs including H_2O_2/HNO_3, $H_2O_2/(O_3+NO_2)$, $HCHO/NO_y$, NO_y, and O_3/NO_y during the afternoon time (from 2 to 6 pm, local time). Among these indicators, $PH_2O_2/PHNO_3$ is considered to be the most robust indicator for O_3 sensitivity regime (Zhang et al., 2009; X.H. Liu et al., 2010b). The values of $PH_2O_2/PHNO_3$ less than 0.2 indicate a VOC-limited O_3 chemistry and higher values indicate a NO_x-limited chemistry (Tonnesen and

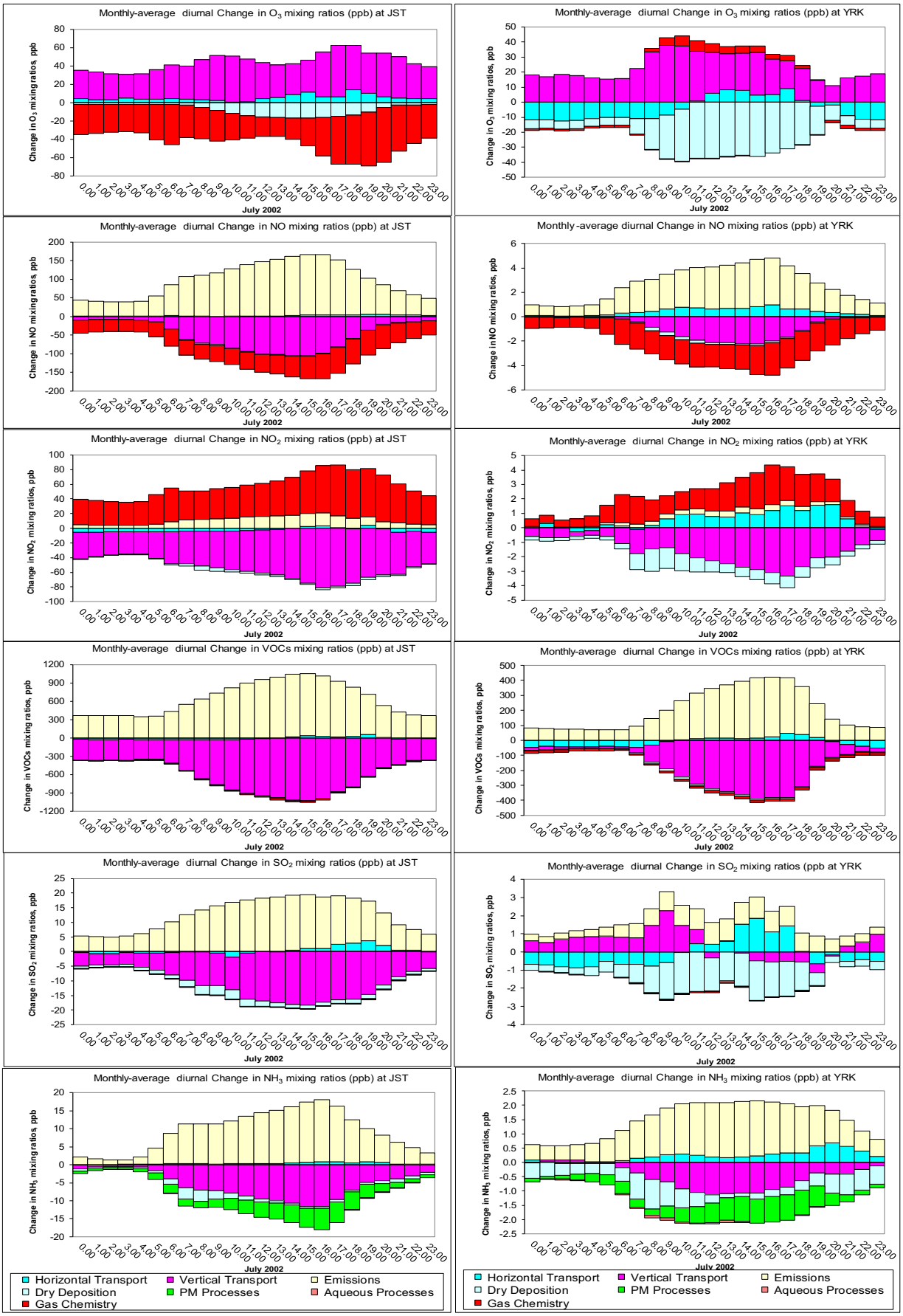

Fig. 4. Monthly-mean diurnal contributions of individual processes to the surface mixing ratios of O_3, NO, NO_2, VOCs, SO_2, and NH_3 at Jefferson Street (JST), Atlanta and Yorkville (YRK), GA in July 2002.

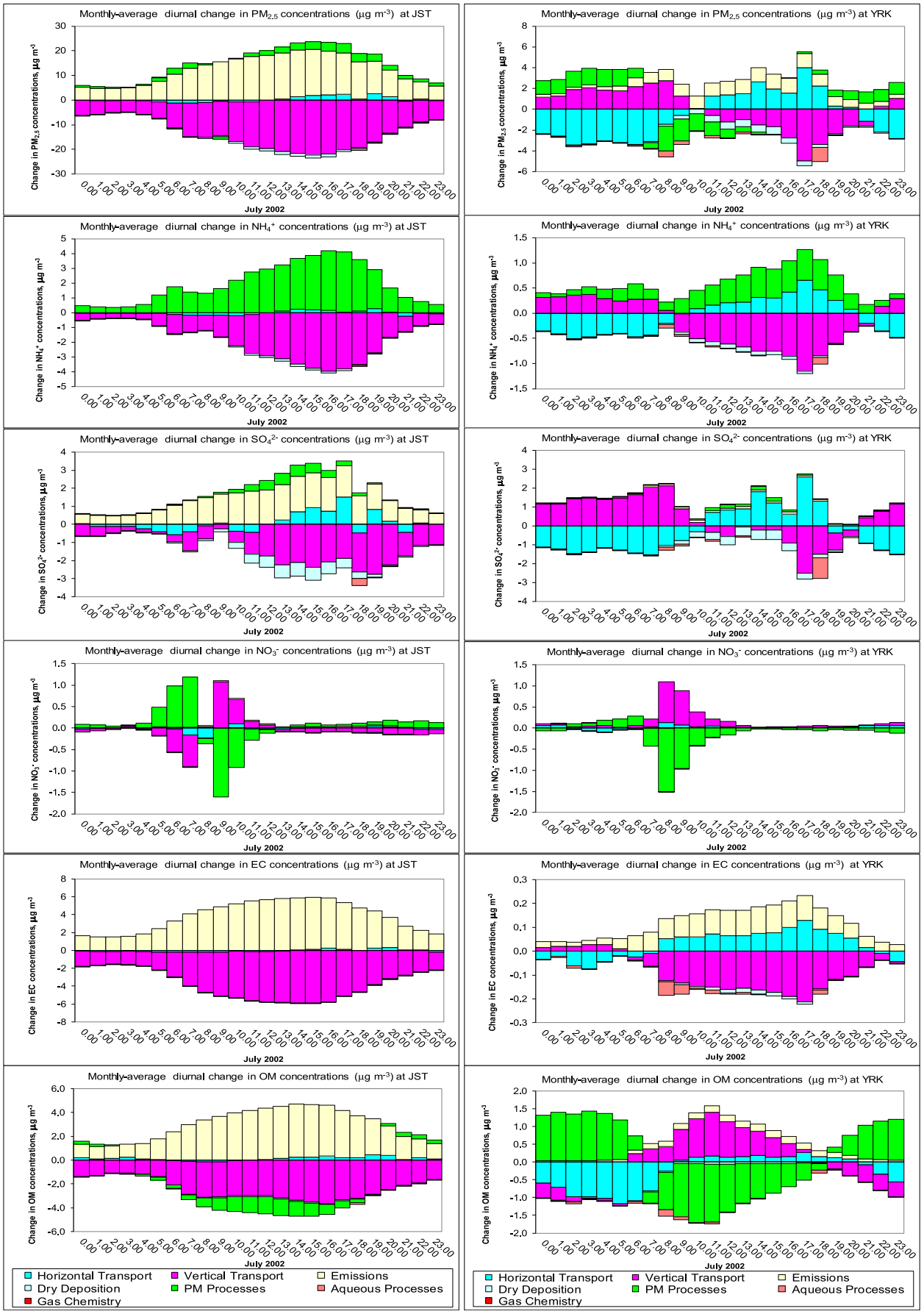

Fig. 5. Monthly-mean diurnal contributions of individual processes to the surface concentrations of $PM_{2.5}$ and its composition including NH_4^+, SO_4^{2-}, NO_3^-, EC, and OM at Jefferson Street (JST), Atlanta and Yorkville (YRK), GA in July 2002.

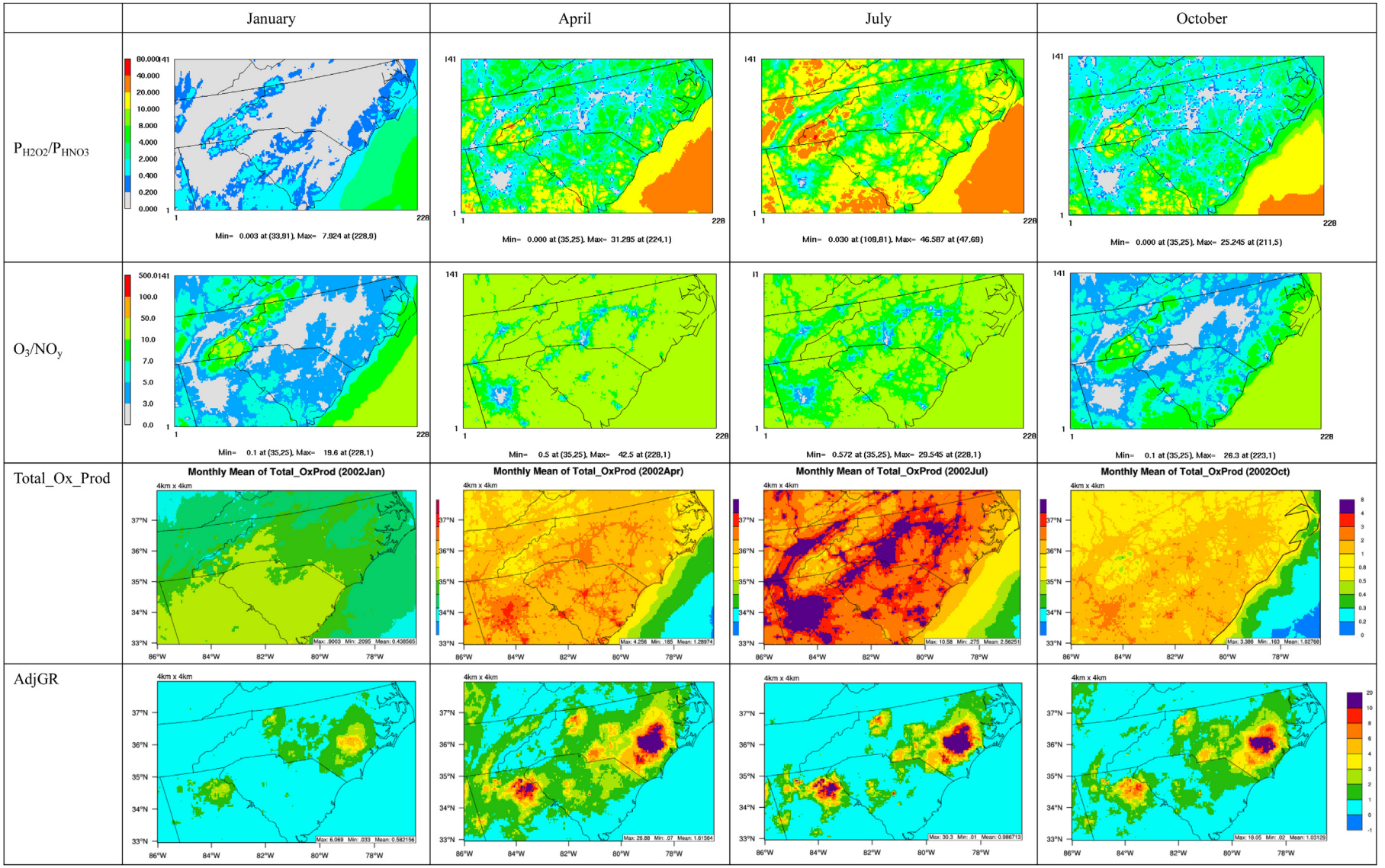

Fig. 6. Spatial distribution of $PH_2O_2/PHNO_3$, O_3/NO_y, Total_Ox_Prod, and AdjGR over the southeastern U.S. during afternoon (2 pm–6 pm, local time) in January, April, July, and October 2002.

Dennis, 2000a). The spatial distribution of $PH_2O_2/PHNO_3$ shows a strong seasonal variation. In January, the values of $PH_2O_2/PHNO_3$ are below 0.2 over the western TN, southern VA and KY, northern GA, and central NC. These regions are urban areas where NO_x emissions from traffic and industrial activities are higher relative to emissions of BVOCs from vegetation in these areas, resulting in VOC-limited O_3 chemistry. Other areas are in NO_x-limited regime due to relatively low NO_x emissions and higher BVOCs emissions. Areas around several large cities, including Raleigh, Greensboro, and Charlotte in NC, Greenville and Anderson in SC, and Atlanta in GA (where O_3 mixing ratios are high) are still under the VOC-limited regime in April, July, and October. Other regions with VOC-limited O_3 chemistry in January switch to the NO_x-limited regime in April, July, and October, due to increased BVOCs emissions in these months. The largest $PH_2O_2/PHNO_3$ values are found over the southern portion of the Great Smoky Mountains, where there is very little influence by anthropogenic NO_x emissions and O_3 chemistry is NO_x-limited. Comparing with the O_3 chemical regimes identified by Zhang et al. (2009) over the continental U.S., these results at 4-km are generally consistent but show much greater details that were not captured by the simulations at 36-km of Zhang et al. (2009). For example, the O_3 chemistry in January over the entire domain used in this work is predicted to be VOC-limited by Zhang et al. (2009) but VOC-limited in most areas and NO_x-limited in some areas by this work. This is most likely due to the use of a coarser horizontal grid resolution of 36-km in Zhang et al. (2009), although the use of a different version of CMAQ and different emissions for a different year (i.e., 2001 in Zhang et al. (2009)) may also help explain these differences. The simulated ratios of $PH_2O_2/PHNO_3$ values are less than 0.2 at JST and YRK in all months, indicating a VOC-limited O_3 chemistry, which is consistent with the results based on the observed indicators in Fig. 1.

The originally proposed transition values are 0.2 for H_2O_2/HNO_3, 0.02 for $H_2O_2/(O_3+NO_2)$, 0.28 for $HCHO/NO_y$, 20 ppb for NO_y, and 7 for O_3/NO_y (Zhang et al., 2009 and references therein). Values less than these thresholds indicate a VOC-limited chemistry and higher values indicate a NO_x-limited chemistry for all indicators except for NO_y (for NO_y, a value greater than 20 ppb means VOC-limited chemistry, otherwise NO_x-limited chemistry). Among these additional indicators, O_3/NO_y is the most robust and indicates O_3 chemical regimes that are consistent with $PH_2O_2/PHNO_3$ without adjusting its thresholds. The threshold values of remaining indicators need to be adjusted. The appropriate transition value for $H_2O_2/(O_3+NO_2)$ may be between 0.01 and 0.02. Adjusting H_2O_2/HNO_3 from 0.2 to 2.4 would make the O_3 chemistry regime closer to $PH_2O_2/PHNO_3$ in July, but does not work in January. Adjusting $HCHO/NO_y$ from 0.28 to 0.14 in January and October and NO_y from 20 to 5 ppb in January and April, would make the O_3 chemistry regimes closer to those indicated by $PH_2O_2/PHNO_3$ in these months. Similar to Zhang et al. (2009) and X.H. Liu et al. (2010b), this study identifies a need for adjustments of transition values of $H_2O_2/(O_3+NO_2)$, H_2O_2/HNO_3, and $HCHO/NO_y$, although different adjusted values are suggested in this work as compared with previous studies. All these studies suggested adjusting NO_y from 20 to 5 ppb. More detailed analyses can be found in the Supplementary material.

4.3. Atmospheric oxidation capacity

As shown in Fig. 6, the values of total_O_x_Pord are the highest in July, and the lowest in January, indicating the highest and lowest atmospheric oxidation capacity, respectively. In July, significant O_x productions occur over the belt of urban areas covering Raleigh and Charlotte in NC, Greenville and Columbia in SC, and Atlanta in the northern GA, indicating a stronger oxidation capacity over urban areas than that over rural areas. In January, total O_x production decreases from the southern states (i.e., GA and SC) to the northern states (i.e., KY and VA) with no obvious differences between urban and rural areas. Fig. S9 shows the spatial distributions of monthly-mean OH_CL, OH_AVOC, and OH_BVOC from IRR output. Seasonal variations of OH_CL are the opposite to the O_x production, with the largest values in January and the lowest values in July (except for urban areas), because a high percentage of OH radicals is converted to HO_2 and RO_2 radicals, which are then removed via HO_2+HO_2 or PAN formation reactions under relatively higher $VOCs/NO_x$ conditions and the oxidation rates of VOCs by OH radicals are stronger in July than that in January. OH radicals reacted with anthropogenic VOCs (OH_AVOCs) and biogenic VOCs (OH_BVOCs) also show strong seasonal variations, with the highest values in July, and the lowest in January.

5. Sensitivity of secondary inorganic PM

Fig. 6 also shows the spatial distributions of monthly-mean AdjGR calculated based on CMAQ predictions. Fig. S10 shows similar plots for DSN and GR. Despite some differences, all three indicators show large areas in NH_3-neutral or NH_3-rich regimes, with the largest areas by AdjGR. All areas having $GR < 0$ now having $0 < AdjGR \leq 1$ and some areas having $0 < GR < 1$ now having $AdjGR \geq 1$ in the four months, reflecting a greater potential for NH_4NO_3 formation over those areas. These results are consistent with Zhang et al. (2009). The largest AdjGR values in the four months occur over the coastal plain of NC over the southeastern NC and a small area in the northeastern of GA, which may be due to high total NH_4^+ in the numerator as results of high agricultural NH_3 emissions and a very small concentration of total nitrate (TNO_3) in the denominator in the calculation of AdjGR.

6. Total nitrogen (N) deposition

N deposition is the pathway of transporting reactive N species from the atmosphere to the biosphere. The pollutants that contribute to N deposition derive mainly from NO_x and NH_3 emissions, which can be controlled. In this study, the deposition fluxes of total N is defined to be a sum of the dry and wet deposition fluxes of oxidized and reduced nitrogen species (NO_y) including NO_3, HNO_3, NH_3, PAN, N_2O_5, HNO_2, HNO_3, NO_3^- and NH_4^+, following Dennis and Mathur (2001) and Pardo et al. (2011). As shown in Fig. 7, total N deposition is estimated to be 0.16–40.8 g N ha^{-1} h^{-1} in 2002, depending on locations and seasons. Relatively larger N deposition fluxes occur in the coastal region of NC and northeastern GA throughout the year. Strong seasonal variations occur, with the highest N deposition fluxes in October and the lowest in January. In January, wet deposition fluxes are larger than dry deposition fluxes over most areas, especially NC, SC, TN, KY and northern GA (Figures not shown). In April and July, dry deposition dominates total N deposition in April and July with ratios larger than 50% over most areas. The total N deposition fluxes in October are higher than those in the other 3 months over most of the domain. Similar to January, wet deposition dominates over dry deposition in most areas. Abundant NH_3 emissions are reported over the southeastern NC (covering Bladen, Duplin, Greene, Lenoir, Sampson, and Wayne counties) caused by the hog population; and over a portion of GA (covering Franklin, Madison, Habersham, and Banks Counties), caused mainly by the explosive growth of the broiler industry in those regions (Stephen and Aneja, 2008). High total N deposition fluxes over the eastern NC and northern GA mainly result from NH_3 deposition due to nearby high NH_3 emissions, while N deposition fluxes in other areas may be dominated by other species such as HNO_3 and NO_x. Fig. 7 also shows the absolute amount of total

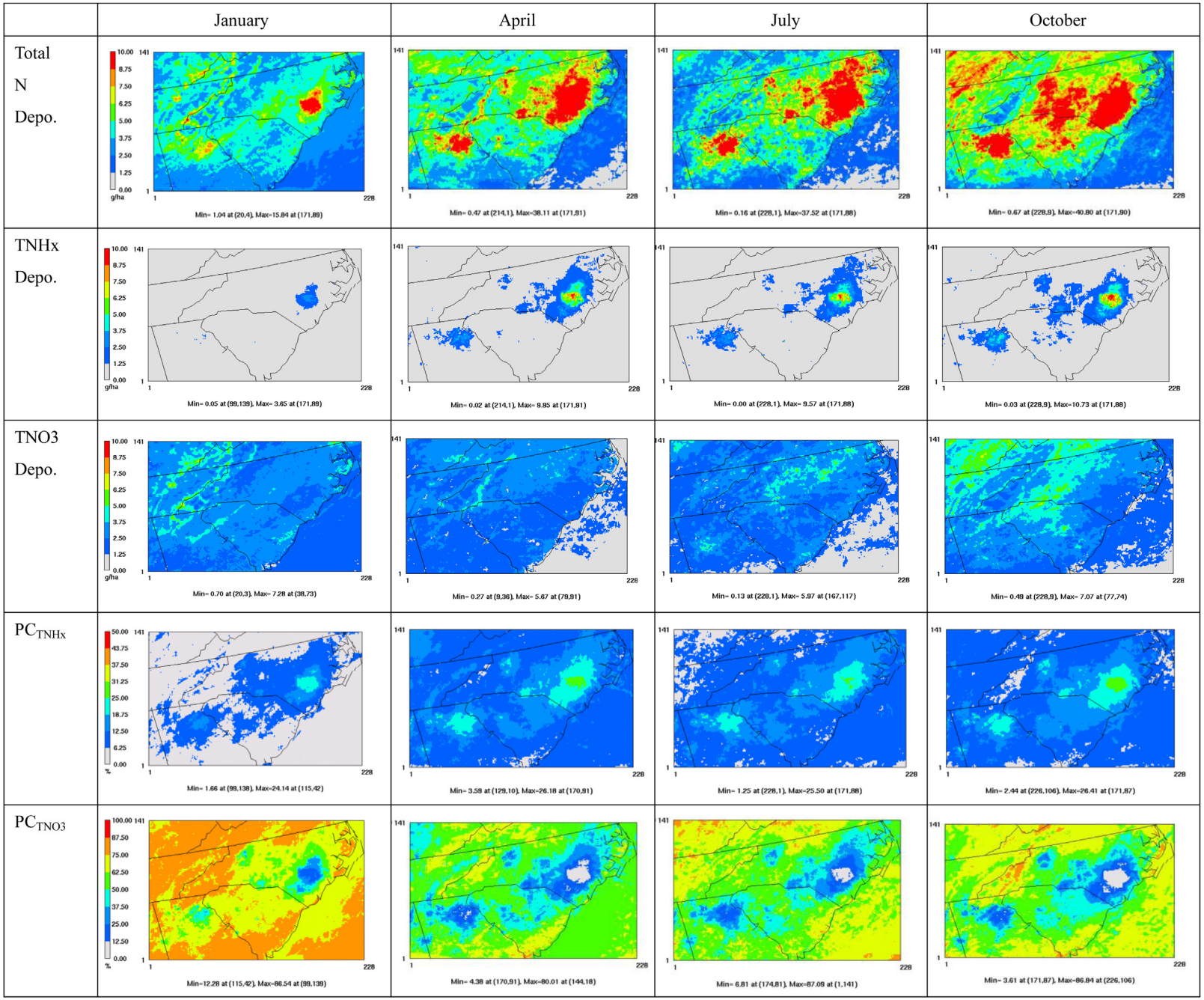

Fig. 7. The total deposition of N, total ammonium ($TNH_x = NH_3 + NH_4^+$), and total nitrate ($TNO_3 = HNO + NO_3^-$) and percentage contributions (PC) of the total deposition of TNO_3 and TNH_x to the total N deposition over the southeastern U.S. in January, April, July, and October 2002.

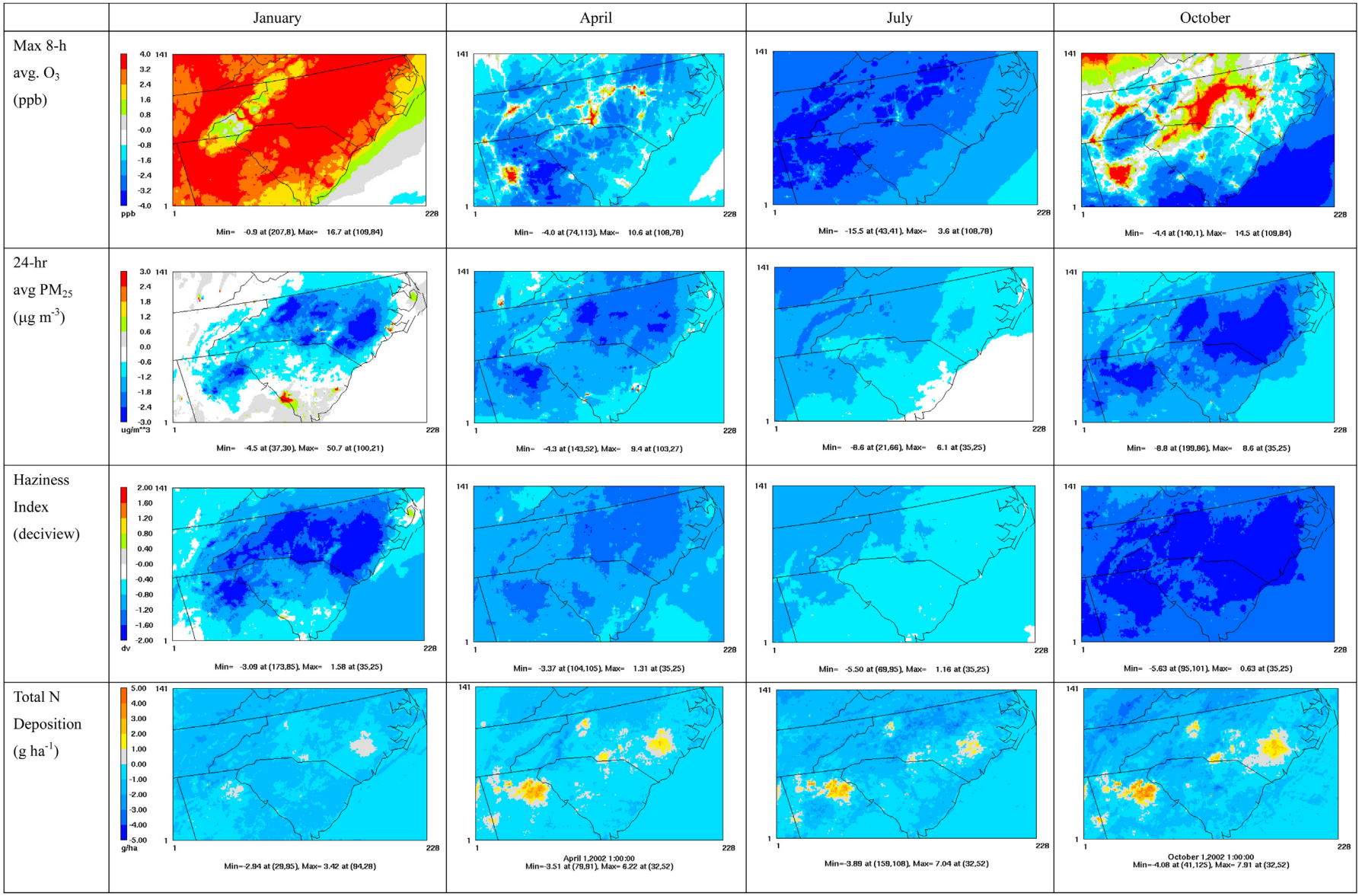

Fig. 8. Absolute differences of the concentration of O_3 and $PM_{2.5}$, haziness index, and total N deposition in January, April, July, and October between 2002 and 2018.

deposition and percentage contributions (PCs) of total NO_3^- ($TNO_3 = HNO_3 + NO_3^-$) and total NH_x ($TNH_x = NH_3 + NH_4^+$) to the total N deposition. For most of the domain, TNO_3 and TNH_x account for 60–80% of the total N deposition, with 1.2–26.4% from TNH_x primarily over NH_3 source regions and 3.6–87.1% from TNO_3 away from the sources. The spatial distributions of PC_{TNO_3} and PC_{TNO_x} are almost the opposite, namely, areas with low PC_{TNO_3} always have high PC_{TNH_x} deposition fluxes. PC_{TNH_x} values are higher (by up to about 18.8–26.4%) over the eastern NC and northeastern GA where PC_{TNO_3} are lower than 10%. This is because most of the NH_3 emissions emitted from hog farms deposit near the source regions and NH_4^+ formed from NH_3 has a longer lifetime than NH_3 and deposits further away from the sources. PC_{TNH_x} are the lowest in January in all months, reflecting the lowest emissions in January. The largest PC_{TNO_3} occur in January, reflecting the impact of meteorological conditions in winter that favors NH_4NO_3 formation.

7. Response of future-year air quality to emission control

Fig. 8 shows the absolute differences of max 8-hr O_3 and $PM_{2.5}$, Haziness index, and total N deposition fluxes between 2002 and 2018. O_3 mixing ratios in January increase over almost the entire domain except for the Great Smoky Mountain regions and some oceanic areas. This is because O_3 chemistry is VOC-limited in January, the effect of NO_x emission reduction dominates over that of the VOCs emission reduction. The increases of O_3 mixing ratios are greater in urban areas than in other regions, with increases of max 8-hr average O_3 up to 3.2–16.7 ppb (>12%). In July, O_3 mixing ratios over the entire domain (except for a small increase in CHA, NC) decrease by up to 2–15.5 ppb for max 8-hr average O_3), due to a NO_x-limited O_3 chemistry. The decreases in the max 8-h average O_3 are up to 6% in several large cities and >18% in the suburban and rural areas. At major urban centers such as Atlanta and CHA where O_3 chemistry is VOC-limited in July, the responses of O_3 depend on two competitive effects, i.e., an increase due to the NO_x emission reductions and a decrease due to the VOCs emission reductions. The former effect slightly dominates over the latter effect at CHA, leading to a small net increase in O_3. The latter effect dominates over the former effect at Atlanta, leading to a net decrease in O_3. Responses of O_3 to emission control in April and October are similar. O_3 mixing ratios increase over urban areas, especially over large cities such as Atlanta and Charlotte, because of VOC-limited O_3 chemistry. Over these urban areas, max 8-h average O_3 mixing ratios increase by up to 10.6 ppb (or by 33.9%) in April, and by up to 14.5 ppb (or by 99.4%) in October. In both months, they decrease over other areas (up to 7.4 ppb for both 1-h and 8-h O_3) due to a NO_x-limited O_3 chemistry. The responses of simulated O_3 to projected emission reductions in 2018 are consistent with the O_3 chemistry regimes indicated by $PH_2O_2/PHNO_3$, $HCHO/NO_y$, NO_y, and O_3/NO_y as shown in Fig. 6 and Fig. S8. Differences in O_3 chemistry regimes in different regions and different seasons lead to different O_3 responses to emission changes in future years. This implies that the current emission control strategies based on the combined rules over the southeastern U.S. may not be suitable for O_3 attainment for urban areas such as Charlotte in all seasons.

Different from O_3, $PM_{2.5}$ concentrations in 2018 decrease over almost the entire domain in the four months, with the highest reduction in October. Spatial distributions are different between July and other months. In January, April, and October, the highest reductions in $PM_{2.5}$ concentrations occur over central and eastern NC and northern GA. In July, more $PM_{2.5}$ reduces in the west of the mountain regions. $PM_{2.5}$ concentrations decrease by 1.8–4.5 μg m^{-3} over most of NC and northwestern GA in January, April, and October, and by < 1.8 μg m^{-3} in the rest of areas. In July, $PM_{2.5}$ reductions are larger than 0.6 μg m^{-3} over the land areas, with the highest reduction of $PM_{2.5}$ (by 4.8–8.6 μg m^{-3}) over the southeastern KY and the western part of Great Smoky Mountains. $(NH_4)_2SO_4$, OC, and light absorbing carbon dominate observed $PM_{2.5}$ concentrations in the southeastern U.S. during summertime (Hand et al., 2011), contributing to the visibility degradation. $PM_{2.5}$ components (figures not shown) show various reduction patterns in different months. In January, April, and October, spatial distributions of NO_3^- and NH_4^+ reduction are more consistent with those of $PM_{2.5}$, β_{ext}, and HI than with other species, with obvious reductions over central and eastern NC and the northern GA. SO_4^{2-} shows obvious reductions over the whole domain in all months, its reduction patterns are closer to $PM_{2.5}$, β_{ext}, and HI, as compared with those of other species in July, indicating that contributions of PM species to visibility and their responses to emission control vary with seasons and locations.

Change in chemical concentrations lead to changes in visibility. A decrease in HI or β_{ext} indicates an improved visibility. The responses of β_{ext} and HI to emission control are overall similar, so only those of HI are shown in Fig. 8. Visibility improvements are found over the eastern and central NC and the northwestern GA in all months, with 18–131 Mm^{-1} reduction in β_{ext} and 1.2–5.6 dv reduction in HI. The responses of visibility exhibit a strong seasonal variation in the rest of areas including the mountain regions in NC, TN and KY, southern VA and GA. Relatively small reductions of β_{ext} and HI are found over these regions in January, April, and October, with β_{ext} reduced by 0–48 Mm^{-1} and HI reduced by 0.4–3.2 dv, while large reductions occur in July (β_{ext} reduced by 12–91 Mm^{-1} and HI reduced by 2–5.5 dv). Spatial distributions of β_{ext} and HI are also different between July and other months. In January, April, and October, the highest reductions occur over central and eastern NC and northern GA, while in July, more reductions occur over the west of the mountain regions.

The predicted total N deposition fluxes in 2018 are in the range of 0.11–43.5 g N ha^{-1} h^{-1}, with the highest N fluxes in the coastal NC and the northern GA. Compared with 2002, the total N deposition fluxes increase (by up to 7.9 g N ha^{-1} hr^{-1}) over the coastal NC and the northern GA due to increased NH_3 emissions and decreased NO_x emissions in all months and decrease (by up to 4 g N ha^{-1} hr^{-1}) over the rest of areas in 2018. Their spatial distribution patterns remain similar to those in 2002. Therefore, NH_3 emissions and resulting concentrations and deposition fluxes would become increasingly important as the emissions of NO_x are projected to decrease and those of NH_3 are expected to continuously increase.

8. Conclusions

CMAQ simulations are conducted at a 4-km horizontal resolution in January, April, July, and October in 2002 and 2018 to examine the mechanisms controlling O_3 and PM and the responses of pollutant concentrations, visibility, and N deposition fluxes to projected anthropogenic emission changes over the southeastern U.S. The model performance for both max 1-h and 8-h O_3 at the 4-km grid resolution is acceptable with NMBs within 13%. The performance of $PM_{2.5}$ is satisfactory in January and October at all sites and in April at the CSN site with NMBs within 19%. Larger NMBs (−57.8% to −33%) occur in April at the IMPROVE sites and in July at all sites, which may be due to the meteorological biases and underestimation of emissions of precursors. Among $PM_{2.5}$ components, the largest biases are found for NO_3^-, especially in July and October. Moderate to large biases also exist in OC and EC in April, July and October and in NH_4^+ at most sites all months. The simulated chemical indicators (i.e., NO_y, O_3/NO_x, and O_3/NO_y) generally agree well with observations. The simulation results at 4-km show some improvement for some species but are not always better than those at 12-km, with higher

sensitivity for $PM_{2.5}$ than O_3 to the grid resolution. This indicates that fine scale modeling at 4-km complements the current SIP modeling effort at 12-km and that the fine scale modeling skill should be continuously improved through improving the accuracies of model inputs (e.g., meteorology, emissions, and ICs and BCs) and model treatments (e.g., NO_3^- and SOA).

Contributions of individual process to surface O_3 and PM formation vary with locations and seasons. Vertical transport plays a dominant role in transporting O_3 in urban, rural, and coastal areas. In mountain regions, O_3 mixing ratios are accumulated mainly through both horizontal and vertical transport. Local O_3 mainly forms via gas-phase chemistry at non-urban sites such as YRK, BFT, and GRS from 8 am to 7 pm. Losses of O_3 are mainly due to gas-phase chemistry via NO titration in urban areas and dry deposition and transport processes in rural and mountain areas. Primary emissions and PM processes are major contributors to $PM_{2.5}$ formation, and vertical and horizontal transport contribute to $PM_{2.5}$ loss in urban areas. Transport, emissions, and PM processes influence PM concentrations in rural areas. PM concentrations at Mountain sites are mainly controlled by horizontal and vertical transport. Among all processes studied, cloud processes appear less important for the episodes simulated in this work. While process analyses are consistent with current understanding of major atmospheric processes and their impacts on key pollutants, they are subject to the limitations and uncertainties of the model used.

The surface O_3 chemical regime in the four months is analyzed using several indicators. Based on the indicator of $PH_2O_2/PHNO_3$, the O_3 chemistry in urban areas is VOC-limited throughout the whole year due to relatively high NO_x emissions and low VOC/NO_x ratios, while that in the mountain regions and southern GA is under NO_x-limited due to high BVOCs emissions. The O_3 chemistry in the remaining areas shows seasonal variations with VOCs-limited in January and NO_x-limited in April, July, and October. These results are generally in agreement with the O_3 chemistry regimes indicated by observed indicators of NO_y, O_3/NO_x, and O_3/NO_y at JST and YRK (with exceptions on some days at YRK). Among all photochemical indicators examined, $PH_2O_2/PHNO_3$and O_3/NO_y are the most robust indicators. The chemical regimes indicated by them are consistent with the responses in O_3 mixing ratios to projected emission changes in 2018. The indicators, $HCHO/NO_y$, NO_y, and H_2O_2/HNO_3 can also be used but with adjusted threshold values, although they are not as robust as $PH_2O_2/PHNO_3$ and O_3/NO_y. $H_2O_2/(O_3+NO_2)$ is not recommended to be a photochemical indicator, due to a large inconsistency with chemical regimes indicated by other indicators. The entire domain is under the NH_3-neutral or NH_3-rich condition based on AdjGR, indicating potential NH_4NO_3 formation in most of the southeastern U.S. in the four months. PM formation is sensitive to the emissions of its major precursors including SO_2, NO_x, and NH_3. The highest N deposition fluxes occur in the coastal areas of NC and northern GA throughout 2002. The deposition of TNO_3 and TNH_x contribute more than 80% of total N deposition in the four months. Dry deposition fluxes are larger in April and July but smaller in January and October than wet deposition fluxes over most of the domain.

The projected emission control in 2018 would have important effects on O_3 and $PM_{2.5}$ levels, visibility, and total N deposition over the southeastern U.S. Due to the projected reductions of anthropogenic emissions and the NO_x-limited O_3 chemistry over most areas, O_3 mixing ratios decrease over almost the entire domain in July. In April and October, O_3 mixing ratios increase over almost the entire domain in January and over urban areas in April and October due to a VOC-limited O_3 chemistry. They decrease over non-urban areas in April and October. $PM_{2.5}$ concentrations, β_{ext}, and HI in 2018 decrease over almost the entire domain in all months with the largest reduction in July. The total N deposition in 2018 decreases over most areas except for the central and eastern NC and northern GA where large increases occur due to projected increased NH_3 emissions, indicating that the total N deposition is dominated by NH_3 deposition and the reduction of NO_x emissions does not lead to the reduction of total N deposition.

Air quality in the simulated region would generally be improved in 2018 due to projected reductions in anthropogenic emissions. However, more considerations should be included in the development of the emission control strategies. For example, reducing O_3 mixing ratios in urban areas would require continuous attention on the reductions of both VOCs and NO_x emissions. NO_x reduction may not be effective in reducing O_3 in rural areas or downwind regions, especially in cold weather, due to a VOC-limited O_3 chemistry. A reduction of SO_2 emissions could decrease SO_4^{2-} concentrations but an increase in NH_3 emissions would increase NO_3^- concentrations, despite a reduction of NO_x emissions. One limitation of this study is the use of the same meteorological inputs in 2018 and 2002, although it avoids complexities caused by meteorological variability and allows a focused study on the impact of projected emission changes on future air quality. Future work should consider changes in both emissions and climate in future years, because climate changes may compensate some changes by anthropogenic emissions.

Acknowledgments

This project is supported by National Research Initiative Competitive Grant no. 2008-35112-18758 from the USDA Cooperative State Research, Education, and Extension Service Air Quality Program. Thanks are due to Pat Brewer, Mike Abraczinskas, Hoke Kimball, and Wayne Cornelius, NC Department of Environmental and Natural Resources, for providing 12-km VISTAS CMAQ inputs, outputs, and observations for NC; Don Olerud, Baron Advanced Meteorological Systems, for providing 12-km MM5 outputs; Dennis McNally and Cyndi Loomis, Alpine Geophysics, Inc., for providing the source code of the CMAQ v4.51 with SOA modules and updated VISTAS emission inventories; Kristen Olsen, a former student of NCSU, for conducting January and July 2002 simulations; and Kai Wang, a post-D researcher at NCSU, for making some plots.

Appendix A. Supplementary data

Supplementary data related to this article can be found at http://dx.doi.org/10.1016/j.atmosenv.2013.03.057.

References

American Lung Association, State of the Air, 2011. http://www.stateoftheair.org/2011, (accessed 09.09.12.).

Appel, K.W., Foley, K.M., Bash, J.O., Pinder, R.W., Dennis, R.L., Allen, D.J., Pickering, K., 2011. A multi-resolution assessment of the Community Multiscale Air Quality (CMAQ) model v4.7 wet deposition estimates for 2002–2006. Geoscientific Model Development 4, 357–371. http://dx.doi.org/10.5192/gmd-4-357-2011.

Arunachalam, S., Holland, A., Do, B., Abraczinskas, M., 2006. A quantitative assessment of the influence of grid resolution on predictions of future-year air quality in North Carolina, USA. Atmospheric Environment 40, 5010–5026.

Baek, J., Hu, Y., Odman, M.T., Russell, A.G., 2011. Modeling secondary organic aerosol in CMAQ using multigenerational oxidation of semi-volatile organic compounds. Journal of Geophysical Research 116, D22204. http://dx.doi.org/10.1029/2011JD015911.

Burr, M.B., Zhang, Y., 2011. Source apportionment of $PM_{2.5}$ over the eastern U.S., Part II: source apportionment simulations using CAMx/PSAT and comparisons with CMAQ source sensitivity simulations. Atmospheric Pollution Research 2, 318–336.

Byun, D., Schere, K.L., 2006. Review of the governing equations, computational algorithms, and other components of the models 3- Community Multiscale Air Quality (CMAQ) modeling system. Applied Mechanics Reviews 59, 51–77.

Carlton, A.G., et al., 2010. To what extent can biogenic SOA be controlled? Environmental Science and Technology 44, 3376–3380.

Chameides, W.L., Cowling, E.B., 1995. The State of the Southern Oxidants Study: Policy Relevant Scientific Findings in Ozone Pollution Research 1988–1994. Southern Oxidants Study, N.C. State University, Raleigh, p. 133.

Chuang, M.T., Zhang, Y., Kang, D.W., 2011. Application of WRF/Chem-MADRID for real-time air quality forecasting over the Southeastern United States. Atmospheric Environment 45, 6241–6250.
Civerolo, K.L., Hogrefe, C., Lynn, B., Rosenzweig, C., Goldberg, R., Rosenthal, J., Knowlton, K., Kinney, P.L., 2008. Simulated effects of climate change on summertime nitrogen deposition in the eastern US. Atmospheric Environment 42, 2074–2082.
Dennis, R.L., Mathur, R., 2001. In: Medina, Miquel A., Kabala, Zbigniew J. (Eds.), Airshed Domains for Modeling Nitrogen Atmospheric Deposition of Oxidized and Reduced Nitrogen to the Neuse/Pamlico System of North Carolina. Hydrological Science and Technology 17 (1–4), 107–117.
Dennis, R.L., Mathur, R., Pleim, J.E., Walker, J.T., 2010. Fate of ammonia emissions at the local to regional scale as simulated by the Community Multiscale Air Quality model. Atmospheric Pollution Research 1, 207–214.
Eder, B., Shaocai, Yu, 2006. An evaluation of model performance of EPA models-3/CMAQ. Atmospheric Environment 40, 4811–4824.
Edgerton, E.S., Hartsell, B.E., Saylor, R.D., Jansen, J.J., et al., 2006. The southeastern Aerosol Research and characterization study: Part III. Continuous measurements of fine particulate matter mass and composition. Journal of the Air & Waste Management Association 56, 1325–1341.
Goldstein, A.H., et al., 2009. Biogenic carbon and anthropogenic pollutants combine to form a cooling haze over the southeastern United States. Proceedings of the National Academy of Sciences of the United States of America 106, 8835–8840.
Hand, J.L., et al., 2011. IMPROVE – Interagency Monitoring of Protected Visual Environments Report V.
Hansen, D.A., Edgerton, E.S., Hartsell, B.E., Jansen, J.J., Kandasamy, N., Hidy, G.M., Blanchard, C.L., 2003. The southeastern aerosol research and characterization study: part I: overview. Journal of Air & Waste Management Association 53, 1460–1471.
Liu, P., Zhang, Y., Yu, S.C., Schere, K.L., 2010. Use of a process analysis tool for diagnostic study on fine particulate matter predictions in the U.S.-Part II: analyses and sensitivity simulations. Atmospheric Pollution Research 2, 61–71.
Liu, P., Zhang, Y., 2010. Use of a process analysis tool for diagnostic study on fine particulate matter predictions in the U.S. Part I: model evaluation using surface, aircraft, and satellite data. Atmospheric Pollution Research 2, 49–60.
Liu, X.-H., Zhang, Y., Olsen, K., Wang, W.-X., Do, B., Bridgers, G., 2010a. Responses of future air quality to emission controls over North Carolina, Part I: model evaluation for current-year simulations. Atmospheric Environment 44 (23), 2443–2456.
Liu, X.H., Zhang, Y., Xing, J., Zhang, Q., Wang, K., Streets, D.G., Jang, C.J., Wang, W.-X., Hao, J.-M., 2010b. Understanding of regional air pollution over China using CMAQ-Part II. Process analysis and sensitivity study. Atmospheric Environment 44, 3719–3727.
Lu, C.H., Chang, J.S., 1998. On the indicator-based approach to assess ozone sensitivities and emissions features. Journal of Geophysical Research 103, 3453–3462.
MACTEC, Inc., 2008. Documentation of the Base G2 and Best & Final 2002 Base Year, 2009 and 2018 Emission Inventories for VISTAS. report. MACTEC Engineering and Consulting, Inc., Alpharetta, GA.
Milford, J.B., Gao, D.F., Sillman, S., Blossey, P., Russell, A.G., 1994. Total reactive nitrogen (NO_y) as an indicator of the sensitivity of ozone to reductions in hydrocarbon and NO_x emissions. Journal of Geophysical Research 99, 3533–3542.
Morris, R.E., Koo, B., Guenther, A., Yarwood, G., McNally, D., Tesche, T.W., Tonnesen, G., Boylan, J., Brewer, P., 2006. Model sensitivity evaluation for organic carbon using two multi-pollutant air quality models that simulate regional haze in the southeastern United States. Atmospheric Environment 40, 4960–4972.
Odman, M.T., Hu, Y.T., Chang, M.E., Russell, A.G., 2007. Forecasting Ozone and PM2.5 in Southeastern U.S. In: Developments in Environmental Science, vol. 6, pp. 219–228. (Chapter 2.14).
Olerud, D., Sims, A., 2004. MM5 2002 Modeling in Support of VISTAS (Visibility Improvement – State and Tribal Association of the Southeast). report. Baron Advanced Meteorological Systems, LLC, Raleigh, NC. August.
Olsen, K., 2009. Fine Scale Modeling of Agricultural Air Quality over the Southeastern United States: Application and Evaluation of Two Air Quality Models. MS Thesis. NCSU, Raleigh, NC. May.
Pardo, L.H., Fenn, M., Goodale, C.L., Geiser, L.H., Driscoll, C.T., Allen, E.B., Baron, J.S., Bobbink, R., Bowman, W., Clark, C., Emmitt, B., Gilliam, F.S., Greaver, T.L., Hall, S.J., Lilleskov, E.A., Liu, L., Lyncy, J., Nadelhoffer, K., Perakis, S.S., Robin-Abbott, M., Stoddard, J.L., Weathers, K., Dennis, R.L., 2011. Effects of Nitrogen Deposition and Empirical Nitrogen Critical Loads for Ecoregions of the United States. In: Ecological Applications, vol. 21(8). Ecological Society of America, Ithaca, NY, pp. 3049–3082.
Pinder, R.W., Dennis, R.L., Bhave, P.V., 2008. Observable indicators of the sensitivity of PM2.5 nitrate to emission reductions: Part I: derivation of the adjusted gas ratio and applicability at regulatory-relevant time scales. Atmospheric Environment 42 (6), 1275–1286. http://dx.doi.org/10.1016/j.atmosenv.2007.10.039.
Queen, A., Zhang, Y., 2008. Examining the sensitivity of MM5-CMAQ predictions to explicit microphysics schemes and horizontal grid resolutions, Part III—the impact of horizontal grid resolution. Atmospheric Environment 42, 3869–3881.
Seinfeld, J.H., Pandis, S.N., 2006. Atmospheric Chemistry and Physics: From Air Pollution to Climate Change. John Wiley and Sons, Inc, p. 1203.
Sillman, S., 1995. The use of NO_y, H_2O_2, and HNO_3 as indicators for ozone-NO_x hydrocarbon sensitivity in urban locations. Journal of Geophysical Research 100 (D7), 4175–4188.
Sillman, S., He, D.Y., Cardelino, C., Imhoff, R.E., 1997. The use of photochemical indicators to evaluate ozone-NO_x-hydrocarbon sensitivity: case studies from Atlanta, New York, and Los Angeles. Journal of the Air & Waste Management Association 47, 642–652.
Stephen, K., Aneja, V.P., 2008. Trends in agricultural ammonia emissions and ammonium concentrations in precipitation over the Southeast and Midwest United States. Atmospheric Environment 42, 3238–3252.
Tagaris, E., Manomaiphiboon, K., Liao, K.J., Leung, L.R., Woo, J.H., He, S., Amar, P., Russell, A.G., 2007. Impacts of global climate change and emissions on regional ozone and fine particulate matter concentrations over the United States. Journal of Geophysical Research 112, D14312. http://dx.doi.org/10.1029/2006JD008262.
Tonnesen, G.S., Dennis, R.L., 2000a. Analysis of radical propagation efficiency to assess ozone sensitivity to hydrocarbons and NO_x. 2. Long-lived species as indicators of ozone concentration sensitivity. Journal of Geophysical Research 105 (D7), 9227–9241.
Tonnesen, G.S., Dennis, R.L., 2000b. Analysis of radical propagation efficiency to assess ozone sensitivity to hydrocarbons and NO_x: 1. Local indicators of instantaneous odd oxygen production sensitivity. Journal of Geophysical Research 105, 9213–9225. http://dx.doi.org/10.1029/1999JD900371.
Turpin, B.J., Lim, H.-J., 2001. Species contributions to $PM_{2.5}$ mass concentrations: revisiting common assumptions for estimating organic mass. Aerosol Science and Technology 35, 602–610.
U.S. EPA, 2007. Guidance on the Use of Models and Other Analyses for Demonstrating Attainment of Air Quality Goals for Ozone, PM2.5, and Regional Haze. EPA – 454/B-07–002, April.
Wu, S.Y., Hu, J.L., Zhang, Y., Aneja, V.P., 2008. Modeling atmospheric transport and fate of ammonia in North Carolina, part II: effect of ammonia emissions on fine particulate matter formation. Atmospheric Environment 42, 3437–3451.
Yu, S.C., Dennis, R., Roselle, S., Nenes, A., Walker, J., Eder, B., Schere, K., Swall, J., Robarge, W., 2005. An assessment of the ability of 3-D air quality models with current thermodynamic equilibrium models to predict aerosol NO_3^-. Journal of Geophysical Research 110, D07S13 http://dx.doi.org/10.1029/2004JD004718.
Yu, S.C., Mathur, R., Schere, K., 2008. Evaluation of real-time $PM_{2.5}$ forecasts and process analysis for $PM_{2.5}$ formation over the eastern United States using the Eta-CMAQ forecast model during the 2004 ICARTT study. Journal of Geophysical Research 113, D06204. http://dx.doi.org/10.1029/2007JD009226.
Yu, S.C., Mathur, R., Schere, K., Kang, D.W., Tong, D., 2009. A study of the ozone formation by ensemble back trajectory-process analysis using the Eta-CMAQ forecast model over the northeastern U.S. during the 2004 ICARTT period. Atmospheric Environment 43, 355–363. http://dx.doi.org/10.1016/j.atmosenv.2008.09.079.
Zhang, Y., Hu, X.M., Leung, R., Gustafson Jr., W.I., 2008. Impacts of regional climate change on biogenic emissions and air quality. Journal of Geophysical Research 113, D18310. http://dx.doi.org/10.1029/2008JD009965.
Zhang, Y., Liu, P., Pun, B., Seigneur, C., 2006a. A comprehensive performance evaluation of MM5-CMAQ for the summer 1999 southern oxidants study episode, part-i. Evaluation protocols, databases and meteorological predictions. Atmospheric Environment 40, 4825–4838.
Zhang, Y., Liu, P., Queen, A., Misenis, C., Pun, B., Seigneur, C., Wu, S.-Y., 2006b. A comprehensive performance evaluation of MM5-CMAQ for the summer 1999 southern oxidants study episode-Part II: gas and aerosol predictions. Atmospheric Environment 40, 4839–4855.
Zhang, Y., Liu, P., Pun, B., Seigneur, C., 2006c. A comprehensive performance evaluation of MM5-CMAQ for summer 1999 southern oxidants study episode, Part III. Diagnostic and mechanistic evaluations. Atmospheric Environment 40, 4856–4873.
Zhang, Y., Liu, X.H., Wang, W.X., Do, B., Bridgers, G., 2010. Responses of future air quality to emission controls over North Carolina, Part II: analyses of future-year predictions and their policy implications. Atmospheric Environment 44, 2767–2779.
Zhang, Y., Pun, B., Wu, S.Y., Vijayaraghavan, K., Seigneur, C., 2004. Application and evaluation of two air quality models for particulate matter for a Southeastern U.S episode. Journal of Air & Waste Management Association 54, 1478–1493.
Zhang, Y., Wen, X.Y., Wang, K., Vijayaraghavan, K., Jacobson, M.Z., 2009. Probing into regional O_3 and particulate matter pollution in the United States: 2. An examination of formation mechanisms through a process analysis technique and sensitivity study. Journal of Geophysical Research 114, D22305. http://dx.doi.org/10.1029/2009JD011900.